A new pterodactyloid pterosaur with a unique filter-feeding apparatus from the Late Jurassic of Germany

David M. Martill[1] · Eberhard Frey[2] · Helmut Tischlinger[3,4] · Matthias Mäuser[5] · Héctor E. Rivera-Sylva[6] · Steven U. Vidovic[1,7]

Abstract

A new long-legged, spatula-beaked, filter-feeding pterodactyloid pterosaur from Upper Jurassic plattenkalk limestones at Wattendorf, Bavaria, Southern Germany, is remarkable for its completeness, unusual dentition and hints of the preservation of soft tissues, including wing membranes. The fully articulated specimen displays both jaws each side with over one hundred sub-parallel-sided teeth with a small, slightly hooked expansion at the crown tip. There are at least 480 teeth in total. The tip of the rostrum widens to a spatula-like, laterally concave structure with teeth only along its lateral margins. The straight anterior margin is devoid of teeth allowing plankton-rich water to stream in, while the teeth interdigitate forming a fine mesh trap. A slightly up swept rostrum assisted filtering by probable pulsating movements of the long neck, while wading or swimming through shallow water.

Keywords Pterosauria · Ctenochasmatidae · Jurassic · Lagerstätte · Filter-feeding · Germany

Communicated by Handling Editor: Ursula Göhlich.

Deceased: Matthias Mäuser.

✉ David M. Martill
  david.martill@port.ac.uk

1 School of the Environment, Geography and Geosciences, University of Portsmouth, Burnaby Road, Portsmouth PO1 3QL, UK

2 Sonnenbergstraße 27, 75180 Pforzheim, Germany

3 Tannenweg 16, 85134 Stammham, Germany

4 Jura-Museum Eichstätt, Willibaldsburg, 85072 Eichstätt, Germany

5 Staatliche naturwissenschaftliche Sammlungen BayernsNaturkunde-Museum Bamberg, Fleischstr. 2, 96047 Bamberg, Germany

6 Departamento de Paleontología, Museo del Desierto, Blvd. Carlos Abedrop Dávila 3745, Parque Las Maravillas, 25022 Saltillo, Coah., Mexico

7 Open Research & Publication Practice, Library, University of Southampton, University Road, Highfield, SO17 1BJ Southampton, UK

Introduction

The Upper Jurassic laminated limestones of the Franconian Jura in Bavaria, southern Germany, have long been famous for the abundance, diversity and exceptional quality of preservation of their pterosaur fossils (Tischlinger and Frey 2013, 2015 and references therein). Since the first pterosaur was described from there in the eighteenth century by Collini (1784), hundreds of remains of these flying reptiles have been discovered, making the quarries of the Southern Franconian Alb, and especially near Solnhofen, Eichstätt, Mühlheim and Painten the richest Jurassic pterosaur locality in the world (e.g., Wellnhofer 1991; Witton 2014; Ösi et al. 2010; Tischlinger and Frey 2015). *Rhamphorhynchus* (Rhamphorhynchidae) and *Pterodactylus* (Pterodactylidae) are the most common genera and are known from dozens of specimens (Hone et al. 2013; Vidovic and Martill 2014). Indeed, for some taxa, such as *Rhamphorhynhus* and *Pterodactylus*, near complete ontogenetic sequences are known (Wellnhofer 1970; Bennett 1995, 1996, 2007).

UV imaging methods have been used successfully in the study of fossils from the Franconian Jura including pterosaurs, clarifying as well as revealing for the first time a wide and hitherto unknown range of osteological and soft tissue information (Frey et al. 2003a; Tischlinger 2002; Tischlinger
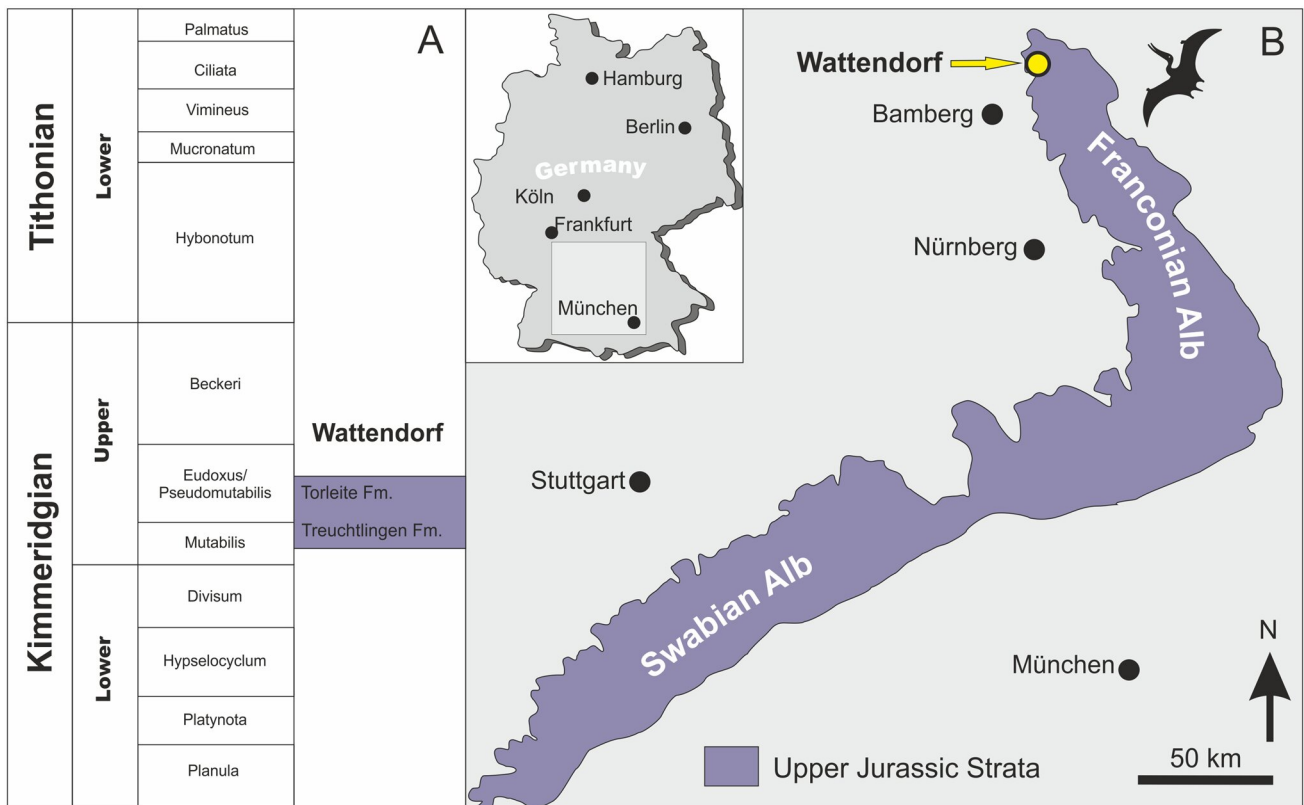
			Wattendorf	
Tithonian	Lower	Palmatus		
		Ciliata		
		Vimineus		
		Mucronatum		
		Hybonotum		
Kimmeridgian	Upper	Beckeri		
		Eudoxus/ Pseudomutabilis	Torleite Fm.	
		Mutabilis	Treuchtlingen Fm.	
	Lower	Divisum		
		Hypselocyclum		
		Platynota		
		Planula		

and Frey 2013). Notably, soft tissue head crest structures have been discovered in *Pterodactylus* sp. as has webbing between the toes (Frey et al. 2003b).

The ecomorphological diversity of pterosaurs from the Franconian Jura ranges from generalists like *Scaphognathus* and *Pterodactylus* to a number of apparent specialist feeders. These include possible aerial insectivores like *Anurognathus* or dip fishing *Rhamphorhynchus* (e.g., Bestwick 2018) to the filter-feeding ctenochasmatids *Ctenochasma* and *Gnathosaurus* with their fine and slender, densely packed teeth (Zhou et al. 2017). Here, we describe a new and hitherto unique filter-feeding pterosaur from the Bavarian Upper Jurassic Wattendorf laminated limestone with the most enigmatic dentition of all pterosaurs known to date.

Locality and context of discovery

The specimen was collected from the quarry of Andreas Schorr GmbH & Co. KG close to the village of Wattendorf in northern Bavaria (Fig. 1). The quarry is located at the northern end of the plateau of the Franconian Alb ("Obermain-Alb") just to the north-west of the village at 50° 02′ 17″ N 11° 06′ 57″ E and covers an area of about 0·3 km^2. The specimen was recovered from spoil dumps in September 2011 following a scientific excavation campaign on the Wattendorf Lagerstätte. The discovery was made accidently while collecting a large block of rudite limestone containing bones of crocodylomorphs.

The first fragment of palm size was found in a spoil heap close to the main excavation level. A single slab fragment, when viewed under low angle light, revealed the articular area between the metacarpus and basal wing-finger phalanx (WP). Because the fragment had sharp, clean edges a thorough search of the spoil heap revealed almost all of the specimen. Only a fragment containing the left metacarpal articulation with WP I of the wing-finger and one fifth of the left ilium is missing. Small fragments of the specimen were found at night by prospecting with a UV lamp.

Geological setting and age

The Wattendorf quarry exposes a series of Late Jurassic limestones of the Treuchtlingen and Torleite formations of the Solnhofen Limestone Group (Fig. 1A). These have been dated as ranging from the upper Mutabilis ammonite biozone to the early Beckeri ammonite Biozone of the Upper Kimmeridgian stage (Zeiss 1977; Niebuhr and Pürner 2014), between 152.1 ± 0.9 and 157.3 ± 1.0 mya (Cohen et al. 2013). The limestones form part of the extensive microbial sponge reef biofacies with intercalated plattenkalks that can be traced from Nusplingen in the southwest to Wattendorf in the northeast (Fig. 1A) and make up the Swabian and Franconian Jura of the Central European carbonate platform (Barthel et al. 1990).

In its northwestern area, the quarry exposes massively bedded Dolomite of the Torleite Formation (Niebuhr and Pürner 2014; Fig. 1A), which dips towards the southeast, forming the base of the "Wattendorf Basin" (Fig. 1B). The base of this basin is filled with well-bedded micritic limestone that includes a sequence of reef-debris, turbidites and platy, laminated limestone (plattenkalk). The plattenkalk is rich in fossils including plant remains, numerous invertebrates as well as well-articulated and diverse chondrichthyans, actinopterygians, coelacanths and reptiles. The latter includes rhynchocephalians, ichthyopterygians, sauropterygians, crocodylomorphs and theropod dinosaurs, as well as pterosaurs (Arratia et al. 2015). This wealth of exceptionally well-preserved fossils was surprising for a region some 130 km north of the famous localities on the Southern Franconian Alb around Solnhofen, Eichstätt and Kelheim. Consequently, scientific excavations were launched in order to rescue as many fossils as possible from the industrial scale limestone quarrying. Since 2004, the excavation team of the Bamberg Natural History Museum (Naturkunde-Museum Bamberg) undertook annual excavation campaigns for a period of about five to six weeks each year (Mäuser et al. 2015). These excavations yielded numerous exceptionally well-preserved fossils including—regarding the vertebrates—a diverse assemblage of chondrichthyans and osteichthyans, accompanied by turtles, rhynchocephalians, crocodilians and remains of pterosaurs, namely isolated teeth of rhamphorhynchines. The near complete and fully articulated skeleton of a pterodactyloid pterosaur recovered during the 2011 excavation campaign is described here (Figs. 1, 2, 3, 4, 5).

At Wattendorf, the limestone sequence records a short-lived change from microbial sponge reef facies to plattenkalk facies in a localised depression known as the Wattendorf-Wanne (=Wattendorf-Basin) (Fig. 1B). The plattenkalk facies is extremely restricted, and even within the quarry, it passes laterally on three sides into dolomitic sponge reef facies within just a few hundred metres of the scientific excavation site. To the east, there is an opening to the centre of the Wattendorf Basin suggesting that the exposure in the quarry represents a cove or inlet within the reef system, in which the plattenkalks accumulated.

Fig. 2 *Balaenognathus maeuseri* gen. et sp. nov. (NKMB P2011-633): holotype and only reported specimen, Torleite Formation of Wattendorf (Late Jurassic). Some small gaps in the slab have been infilled with minor restoration of some bones. A portion of the distal extremity of the left metacarpal IV and part of the left anterior ilium process are known to be missing. Some other missing elements (e.g., the pteroids) may be concealed under larger bones

Sedimentation in the Wattendorf Basin began with a dolomite breccia with intercalations of dolobindstone. In the hanging wall, there is a sequence of about 6 m with alternating layers of reef debris with chert nodules, turbidites and plattenkalks. Bioturbation is sparse at the bottom of the unit but increases rapidly in the uppermost metre of the sequence, which consists of a slightly wavy plattenkalk. This sequence thins to zero on topographic highs of the reef. It is overlain by the informally named 'Wattendorf Limestone'.

Examples of the ammonite *Aulacostephanus eudoxus* from the same horizon as the pterosaur demonstrate its early late Kimmeridgian age (Schweigert 2007), making the 'Wattendorf plattenkalk' the oldest of the Jurassic plattenkalks of the Central European carbonate platform. Overlying the topmost plattenkalk is the so-called Wattendorfer Kalk (Wattendorf Limestone), an approximately 30 m thick sequence of very pure micritic limestones, with reef debris. The plattenkalk facies and the overlying 'Wattendorfer Kalk' belong

Fig. 3 *Balaenognathus maeuseri*, gen. et sp. nov. (NKMB P2011-633): UV image

to the Torleite Formation (Zeiss 1977; Niebuhr and Pürner 2014) (Fig. 1A).

Because the pterosaur specimen P2011-633 was discovered ex situ, its original finding horizon was determined on lithological criteria, which fortunately are highly distinctive and restricted to a very narrow part of the stratigraphic sequence exposed in the Wattendorf quarry. The specimen comes from layer 12 of the main excavation level, a plattenkalk unit of just 150 mm thickness, which consists of very fine-grained, graded alternations of microbial bindstone laminae and very thin clay laminae. The specimen was embedded between bindstone layers that split only with difficulty, lies on the underside of layer 12 and is preserved almost complete and in nearly full articulation on a slab measuring 600×470 mm.

Material and methods

Material

The specimen is housed in the Bamberg Natural History Museum under the collection number NKMB P2011-633 and is currently on display. The specimen was added to the
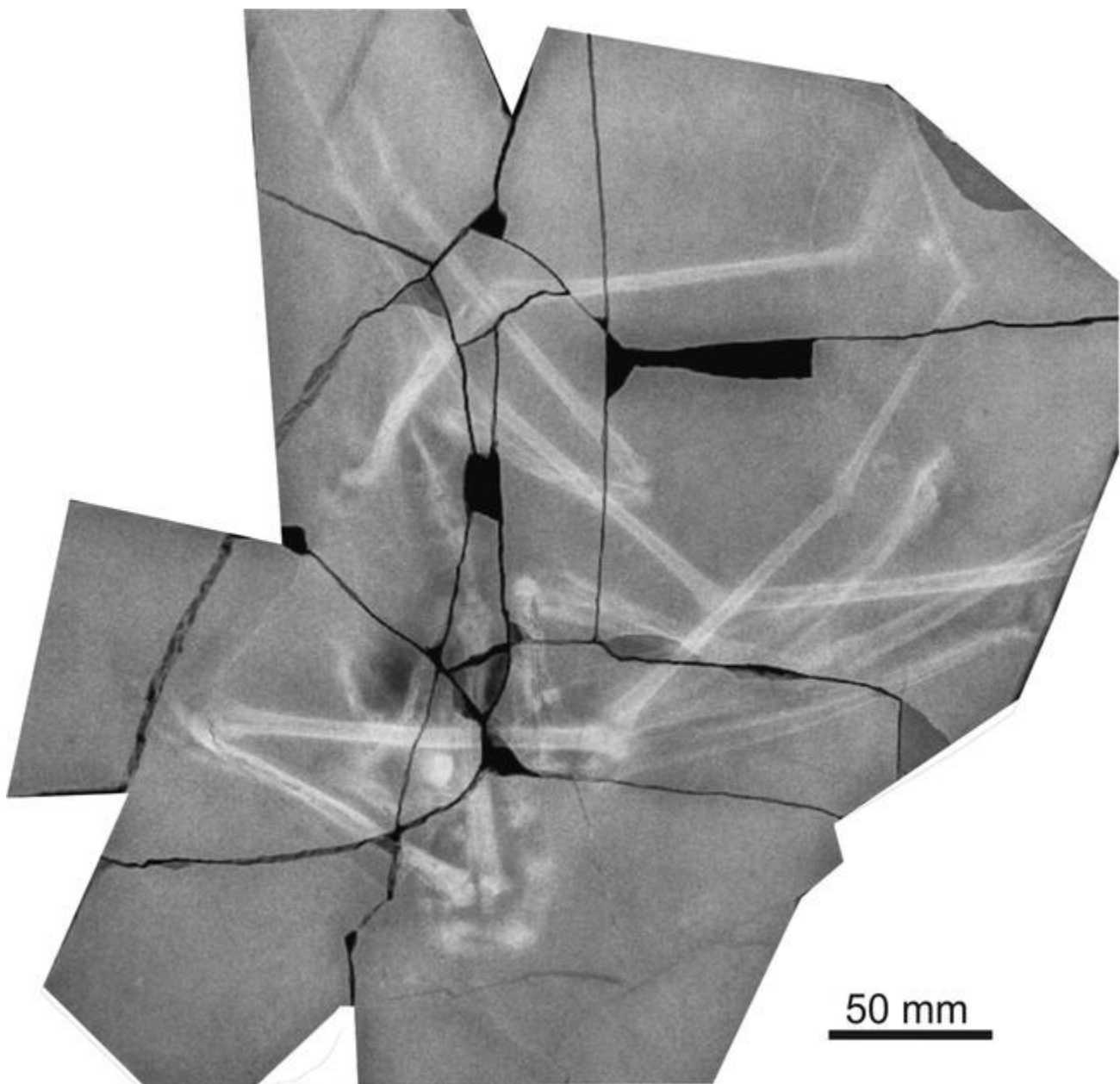
Fig. 4 *Balaenognathus maeuseri* gen. et sp. nov. (NKMB P2011-633): X-ray image of the slab

Bamberg collection on 26.5.2014 under the registration number 02925 as a permanent item of German cultural heritage of national importance under the procedures of the 'Kulturgutschutzgesetz' (a national law for the Protection of Cultural Objects). The specimen described herein will be securely available for the scientific community in perpetuity. The Bavarian State will prevent any potential sale of the fossil.

When discovered, the specimen consisted of a slab broken into 17 pieces (Figs. 2, 3, 4). Despite this damage, the skeleton remained almost complete, because the breaks are mostly clean, and gaps with missing matrix mostly occur beyond the skeleton. Only the distal 'roller' joint of the left wing-finger metacarpal and the articular area of a WP, including the three free digits of the left wing-finger, are missing. A small part of the left ilium is also missing (Figs. 2, 3, 4). The bones present are listed in Table 1.

Preparation and measurements

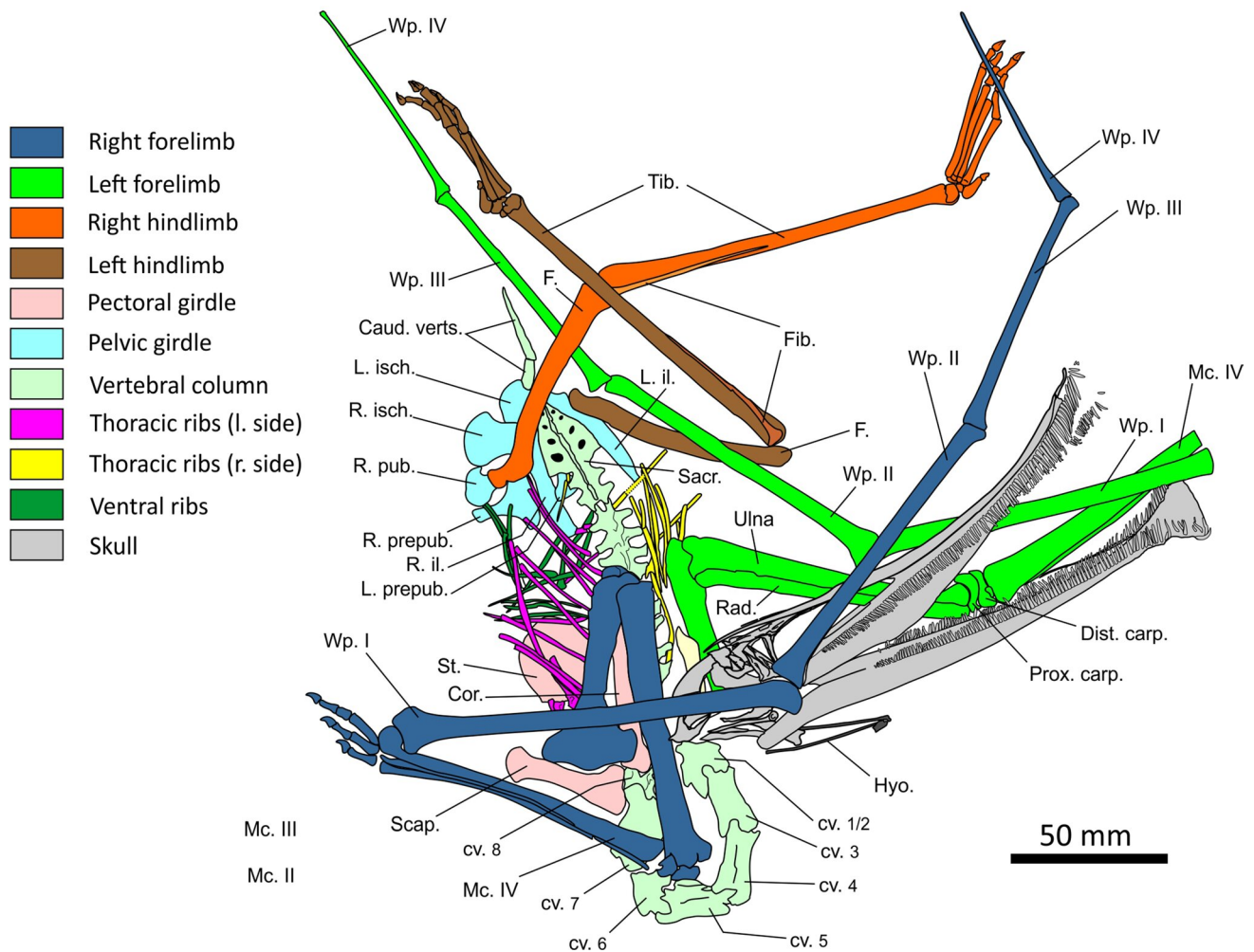The skeleton was prepared by a professional preparator in full relief using Hardy Winkler air scribes and was studied

Fig. 5 *Balaenognathus maeuseri* gen. et sp. nov. (NKMB P2011-633): interpretative drawing. L, left; R, right, Caud. verts., caudal vertebrae; Cor., Coracoid; cv., cervical vertebra; Dist. Carp., distal carpal; F., femur; Fib., Fibula; hu., Humerus; il., Ilium; isch, ischium; Mc., metacarpal; Prox. carp., proximal carpal; pub., pubis; prepub., prepubis; Rad., Radius; Sacr., Sacrum; Scap., scapula; St., sternum; Tib., tibia; Ulna; Wp., wing phalange

using ordinary light, UV light and X-ray. For study under UV the techniques described by Tischlinger (2002, 2015) and Tischlinger and Arratia (2013) were followed. A detailed description of the preparation is given in Völkl-Costantini and Völkl (2013). Measured angles were taken from images imported into CorelDraw and are rounded to the nearest degree. Selected measurements are provided in Table 2.

UV documentation and measurements

Measurements were taken from a high-resolution photograph and were cross-checked with a calibre gauge on the original fossil. The photographs under normal and UV light were taken using Panasonic digital cameras (2×Lumix FZ38). For macro-photography, a Raynox macroscopic lens model M-250 was used together with a Panasonic adapter DMW-LA3.

For UV documentation of the pterosaur, three high intensity Benda UV hand lamps (Type N—16 W) and a wavelength of 365–366 nm (UV-A) were used and mounted at about the same distance around the fossil-bearing slab on tripod mounts. The hand lamps contained 2×8 Watts UV tubes, which provided an even illumination of the 600×600 mm area that included the entire fossil. Depending on the distance of the lamps the illumination intensity ranged from about 1200 to 2500 µW per 10 mm^2.

For the documentation of details, a Labino spotlight beamer (S135, 43/35 W, UV-A-365 nm) was used, which in some cases was equipped with a mid-light reflector to achieve an especially even illumination. According to the manufacturer, this hand UV spot has an illumination intensity of more than 50,000 µW/10 mmm^2 at a distance

of 300 mm. With the mid-light reflector, the illumination intensity is more than 8000 μW/10 mm^2.

Photographs taken under UV light often display a greenish or bluish colour dominance that may mask some features of the fossil. A combination of colour filters and an UV block filter (398 nm) minimized or even eliminated this unwanted effect (see Tischlinger 2002 for details). With the help of filters, the combination of which requires considerable experience and experimentation, all details of the pterosaur skeleton were optimally documented.

Preservation, taphonomy and description of the specimen

The specimen (Figs. 2, 3, 4, 5) is virtually complete and in a high degree of articulation, but most of the bones are crushed flat and have failed in a brittle manner, although some elements exhibit plastic deformation (Figs. 2, 3). Consequently, most bones are fractured, sometimes intensely, and are largely two-dimensional, or almost so. In several places, overlapping parts of the skeleton obscure other bones, notably in the cranium, shoulder region and the posterior end of the pelvis. Nonetheless, much excellent anatomical information can be derived from the specimen, despite bone overlaps and compaction. In the view of the specimen presented in Figs. 2, 3 and 4, the caudal skeleton, sacral region and thorax lie in a nearly straight line and are exposed in dorsal aspect, with some distortion that emphasises the right side of the skeleton. Much of the shoulder girdle and sternum is concealed by bones of the wings and the cervical vertebrae, the latter describing an arc of 180 degrees such that the skull is intimately associated with elements of both wings. Despite this overlap, much of the skull is visible and seen in right lateral aspect (Fig. 6). Oblique flattening means that both rami of the lower jaws are seen, and some of the palatal surface of the rostrum is visible. Teeth of the right dentary are pressed over the left dentary. Bizarrely, the teeth seem to have deformed somewhat plastically (Figs. 6, 7, 8). Consequently, during preparation, some of the teeth 'popped-off' and had to be glued back in place.

The skeleton of the trunk lies slightly on its left side but with the vertebral column of the trunk exposed in dorsal aspect. The entire vertebral column is fully articulated, apart from a small break in the caudal series (Figs. 2, 3, 4, 5). The tail is bent at its base to the left at about 10° but is otherwise straight despite the caudal vertebral column being broken between caudal vertebrae four and five. On the right side of the body, nine ribs are visible. The cranial three overlie the sternum, the internal face of which is visible between the ribs. The right and posterior margins of the bone are exposed. The position of the sternum suggests that its anterior end is still articulated with the coracoids.

On the left side, nine ribs are visible, but they have collapsed over each other. Despite their dislocation, all ribs appear to be at least partially articulated with their respective vertebrae. The left side of the pelvic girdle has been tilted to the right and exposes its right lateral surface, which is still in contact with the sacrum (Figs. 2, 3, 4, 5, 9). The acetabular part is obscured by the head of the right femur that also overlies the medial corner of the right prepubis. The latter bone has rotated about 90° to the right so that the peduncle now faces laterally. The gastralia are disarticulated and scattered in the thoracic region. Seven fragments are preserved with certainty. The left pubis is mostly hidden under the sacrum. Only the iliac blade is seen left to the vertebral column of the trunk and the posteroventral part of the ischium right to the tail base. The left prepubis is hidden beneath the sacrum.

Both humeri are still in articulation with their respective glenoid fossae and face caudally nearly paralleling the vertebral column with a slight lateral rotation (Figs. 2, 3, 4, 5). Both scapulae are present, but only their notarial ends are visible. On the right wing, all bones are articulated with each other, but the articulations between WP I through IV show a hyperextension of about 100° each (Figs. 2, 3, 4, 5, 10). There is an unnatural lateral rotation in the right carpus that resulted in disarticulation of the carpals and an exaggerated angle. The angle between the right humerus and radius/ulna is approximately 24° and that between wing-finger metacarpal and WP I is approximately 60° with both likely reflecting true anatomical positions as does that between WP II and III (Fig. 10).

The right limb is complete and fully articulated but it lies reversed with the knee facing posteriorly (Figs. 2, 3, 4, 5, 10). The head of the femur has become disarticulated from the acetabulum and with its third trochanter covers the tip of the medial flange of the right prepubic bone. The angle between femur and tibia-fibula is 130°. These bones are seen in medial view. The fibula lies in anatomical position. The right pes is seen in dorsomedial aspect (Figs. 2, 3, 4, 5, 11, 12). Metatarsals I–IV and their respective phalanges slightly diverge at angles of about two or three degrees, metatarsal V at an angle of five or six degrees.

The head of the left femur is concealed inside the acetabulum of the left side of the pelvis (Figs. 2, 3, 4, 5). The bone is oriented anterolaterally and describes an angle of about 32° with the vertebral column and is seen from laterally. The tibia is seen in anterolateral aspect and lies flexed at an angle of 46° against the femur. The left pes lies almost straight in line with the tibia and is seen from laterally. Digits II to IV lie parallel with each other, while digit I is slightly abducted at an angle of about 12°.

The skull lies at an angle of approximately 90° to the body thereby contacting the anterior margin of the left scapula with the parietal area (Figs. 2, 3, 4, 5). The occipital condyle has lost contact with the atlas. The quadrate contacts

Fig. 6 *Balaenognathus maeuseri* gen. et sp. nov. (NKMB P2011-633): skull in right lateral view. **A** under ordinary light.; **B** UV image. **C** interpretive drawing; overlying wing bones are in grey. l, left; r, right. hyoids; jug., jugal; lac., lachrymal; lig., supra cranial ligament; max., maxilla; nas., nasal; p., max. premaxilla; par., parietal; qd., quadrate; sq., squamosal; ramus dent., ramus of the dentary
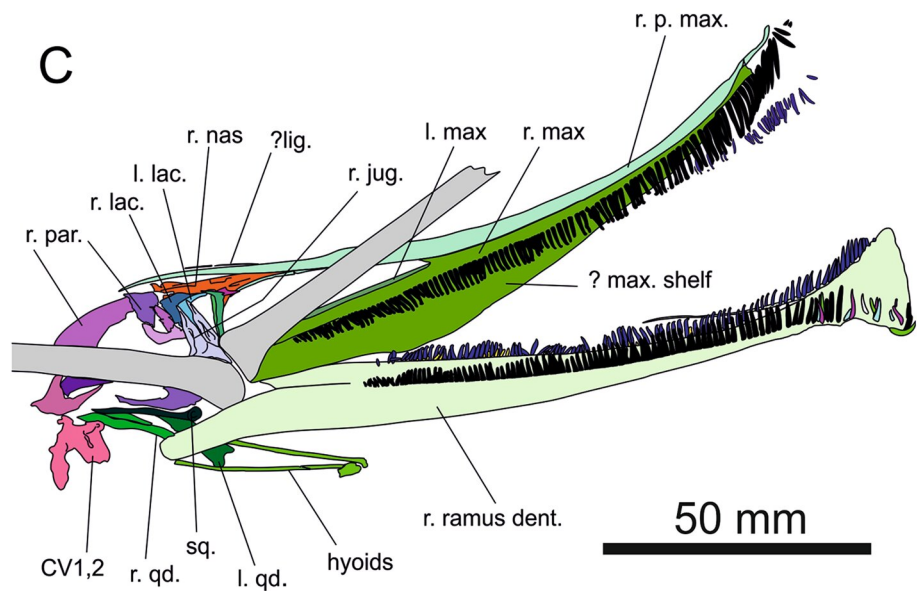
Fig. 7 *Balaenognathus maeuseri* gen. et sp. nov. (NKMB P2011-633): UV images of the teeth. **A** Teeth close to the tip of the maxilla; upper row: labial aspect (right maxilla), lower row: lingual aspect (left maxilla). **B** Close-up of the crown tips of the teeth of the left maxilla showing hook-like modification of the crown tip, seemingly directed anteriorly (arrows). **C** Teeth of the middle part of the dentary (black arrows show the booklets at the crown tip)
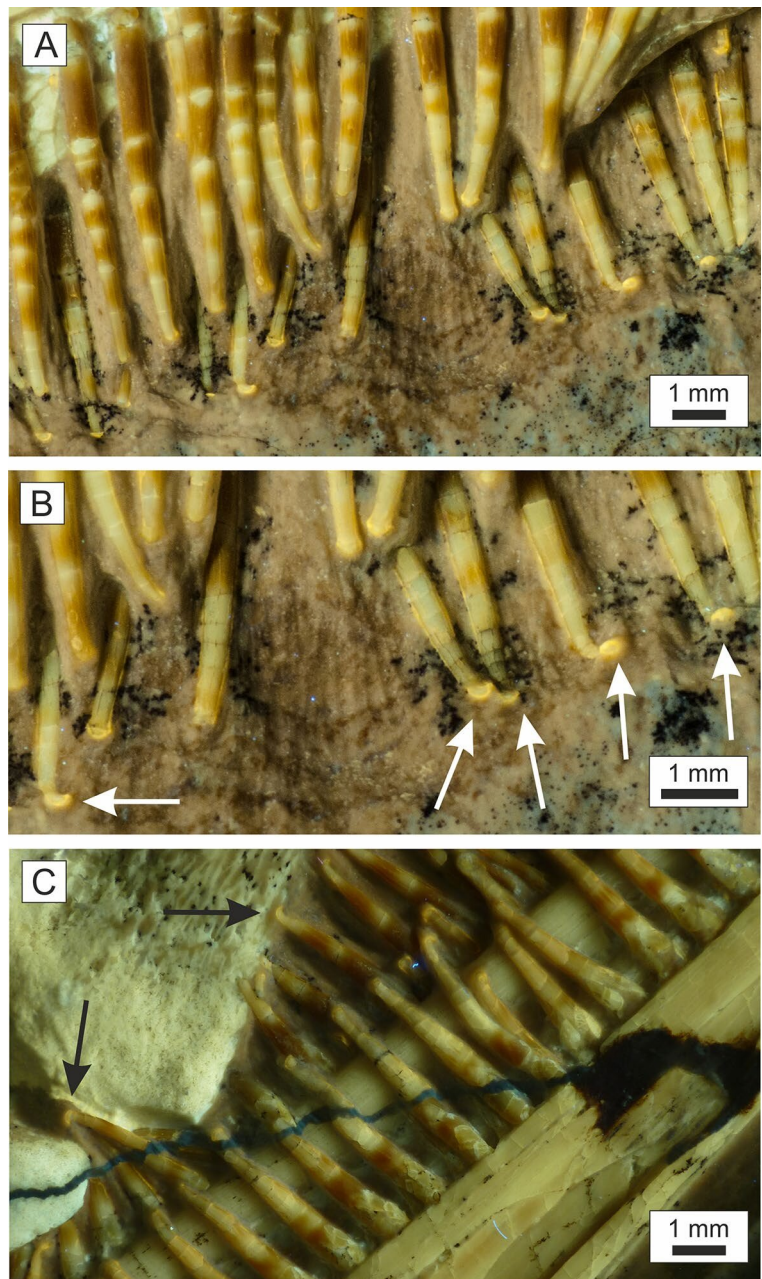

the second cervical vertebra. The skull overlies the distal third of the left radius and ulna and the distal third of WP I. The mandible is articulated with the hyoids contacting its posteroventral end and with its left mandibular ramus lying adjacent to the left wing-finger metacarpal (Figs. 2, 3, 4, 5, 6). The tip of the mandible is slightly distorted to the right because of its triangular expansion, the buccal surface of which is now visible. The tip of the premaxilla is less distorted on its right side. Most of the more than 400 teeth remain in position, even along the margins of the rostral dilatation (Fig. 6).

The following taphonomic scenario for the specimen is proposed. The carcass settled on the sea floor with the right hind limb and the proximal elements of the right wing including the wing-finger metacarpal and the WP I–III. The right WP IV likely projected into the water column for a while prior to settling across the phalanges of the left pes, held in position by the trailing edge of the wing membrane, which, having been still connected the metatarsal V, forced the right hind limb down and rotated it dorsomedially as a complete unit. The skull settled on top of the right wing followed by the trunk, which rolled on its left side guided by the neck that curled. The trunk then swung around the fixed skull and came to rest at an angle of 90° to the skull long axis on its right laterodorsal side. Finally, the left wing settled. During the movement of the trunk, the left hind limb

Fig. 8 *Balaenognathus maeuseri* gen. et sp. nov. (NKMB P2011-633): tooth preservation. **A** UV close-up of the tooth section at the narrowest point of the funnel; the dashed lines connect identical fractures according to their count from the jaw margin, the asterisk marks the tooth depicted in **B**; **B** tooth preservation shown in the interpretive drawing of an isolated tooth
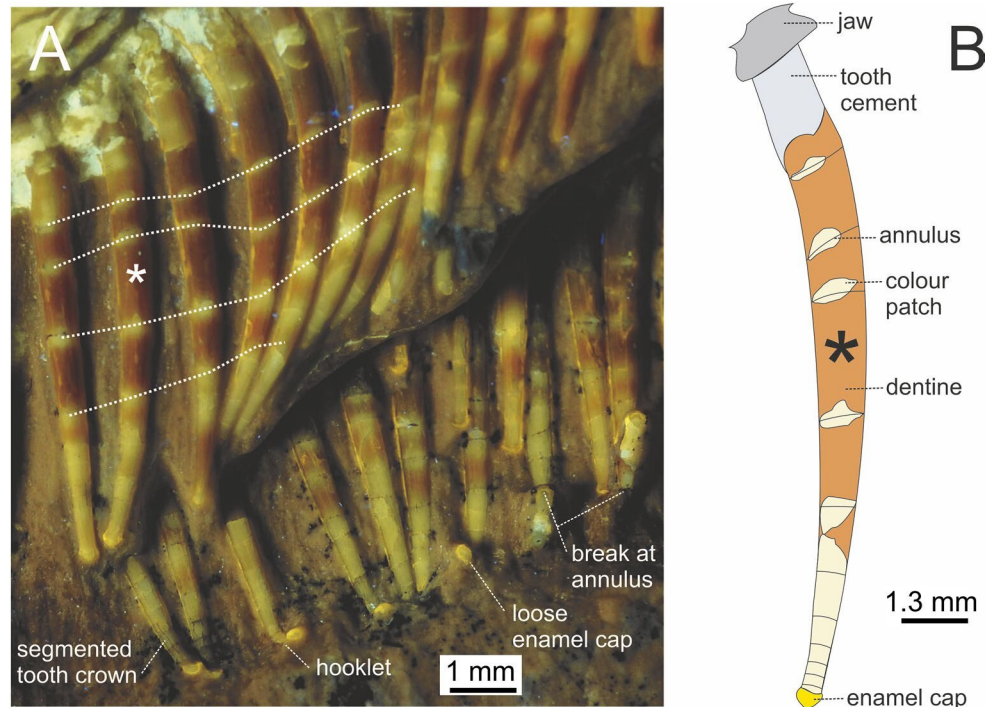
must have been oriented ventrally and allowed the left wing-finger to pass by the femur. Later the femur collapsed across WP II.

The near perfect articulation of the skeleton (Figs. 2, 3, 4, 5) suggests that the carcass must have been at a very early stage of decay with all joints including their ligaments still viable. The disarrangement of the ribs, and especially the abdominal ribs, suggests that the body was bloated by decay gasses while afloat. Likely the rupture of the body wall released the gasses at least partially allowing the carcass to sink. With the release of the internal gas pressure, the sternal plate rotated slightly to the right around its articulation with the coracoids, but the disarticulation of the prepubic bones from the pelvis and the scattered gastralia suggest a rupture in the abdominal area. There is no evidence of predation or scavenging.

Systematic palaeontology

Pterosauria Kaup, 1834
Monofenestrata Lü et al., 2010
Pterodactyloidea Plieninger, 1901
Family **Ctenochasmatidae** Nopcsa, 1928.
Genus *Balaenognathus* n. gen.

Type species. *Balaenognathus maeuseri* n. sp. (see below).

Derivation of generic name. *Balaena* is the generic name of the bowhead whale (*Balaena mysticetus*) a ram filter feeding

cetacean. Thus *balaena* (Latin) for the bowhead whale and gnathus (Latin) for jaw. The genus name refers to the filter mechanism of bowhead whales that have superficially similar feeding strategies.

Diagnosis. See below for type species.

Balaenognathus maeuseri n. g., n. sp.

Derivation of specific name. "*maeuseri*" after our coauthor and good friend Matthias Mäuser who so sadly passed away during the writing of this paper.

Holotype. A single articulated specimen housed at the Naturkunde-Museum Bamberg (Natural History Museum Bamberg) under collection number NKMB P2011-633 (Fig. 2).

Type locality. Quarry of Andreas Schorr GmbH & Co. KG near Wattendorf, Bavaria, Southern Germany (Fig. 1B), at coordinates 50° 02′ 17″ N 11° 06′ 57″ E.

Type horizon and age. Bed 12 of the Wattendorf Plattenkalk, Torleite Formation, *Eudoxus* ammonite Biozone, Upper Jurassic, Upper Kimmeridgian to Tithonian (~ 157–145 mya).

The new specimen is referred to the Ctenochasmatidae according to the following combination of features (Unwin 1995, 2003; Frey and Martill 1998; Kellner 2003):

Fig. 9 *Balaenognathus maeuseri* gen. et sp. nov. (NKMB P2011-633): synsacrum and caudal vertebrae, **A** UV image, **B** line drawing. Overlapping bones and the associated pelvic girdle are shaded grey. l. f., left femur; l. i., left ischium; l. il., left ilium; l. p. p., left prepubis; r.f., right femur; r. i., right ischium; r. il., right ilium; r. p., right pubis; r. p. p., right prepubis; w. p., wing phalanx
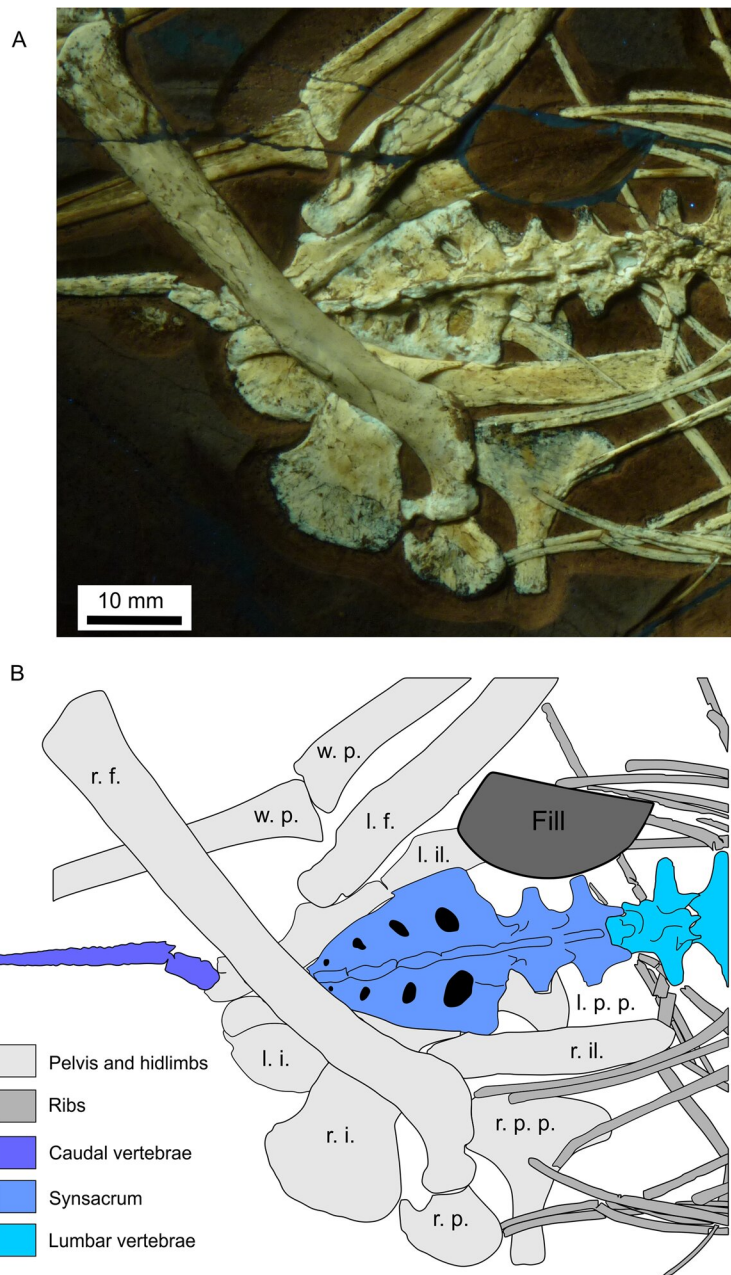
1. Glenoid fossa lies ventral to the vertebral column (Figs. 2, 3; Frey et al. 2003a).
2. Femur longer than humerus (ratio humerus/femur = 0.79; Table 1, Figs. 13, 14).
3. Tibia more than 1/3 longer than femur (ratio femur/tibia = 0.62; Table 1, Fig. 14).
4. Deltopectoral crest situated in the proximal fourth of the humerus and protruding at right angles from the shaft of the humerus; proximal and medial margins of the deltopectoral crest parallel to each other, cranial margin convex (Figs. 2, 3, 4, 5, 10).
5. Sternal plate shovel-shaped (Figs. 2, 3, 4, 5).
6. Cristospine less than 1/5 the length of the sternal plate (not visible on the new specimen).
7. Furca of the coracoid almost twice as wide as the narrowest part of the shaft, which is visible on the right coracoid (Figs. 2, 3, 5)
8. WP II with a sulcus on its ventral face. This groove might be indicative for a crest on the dorsal side, but this is concealed by matrix.

Regarding the ratios of the wing and limb bones (Fig. 13) *Balaenognathus* is unique in the ratio between the length of humerus + radius/ulna + metacarpal IV and the length of the wing-finger. The wing-finger is significantly longer than

Fig. 10 *Balaenognathus maeuseri* gen. et sp. nov.: interpretive drawing of wing skeleton. Dist. syn., distal syncarpal; Hum., humerus; Mc., metacarpal; Prox. syn., Ph., phalanx; proximal syncarpal, for original bones see Figs. 2, 3, and 4
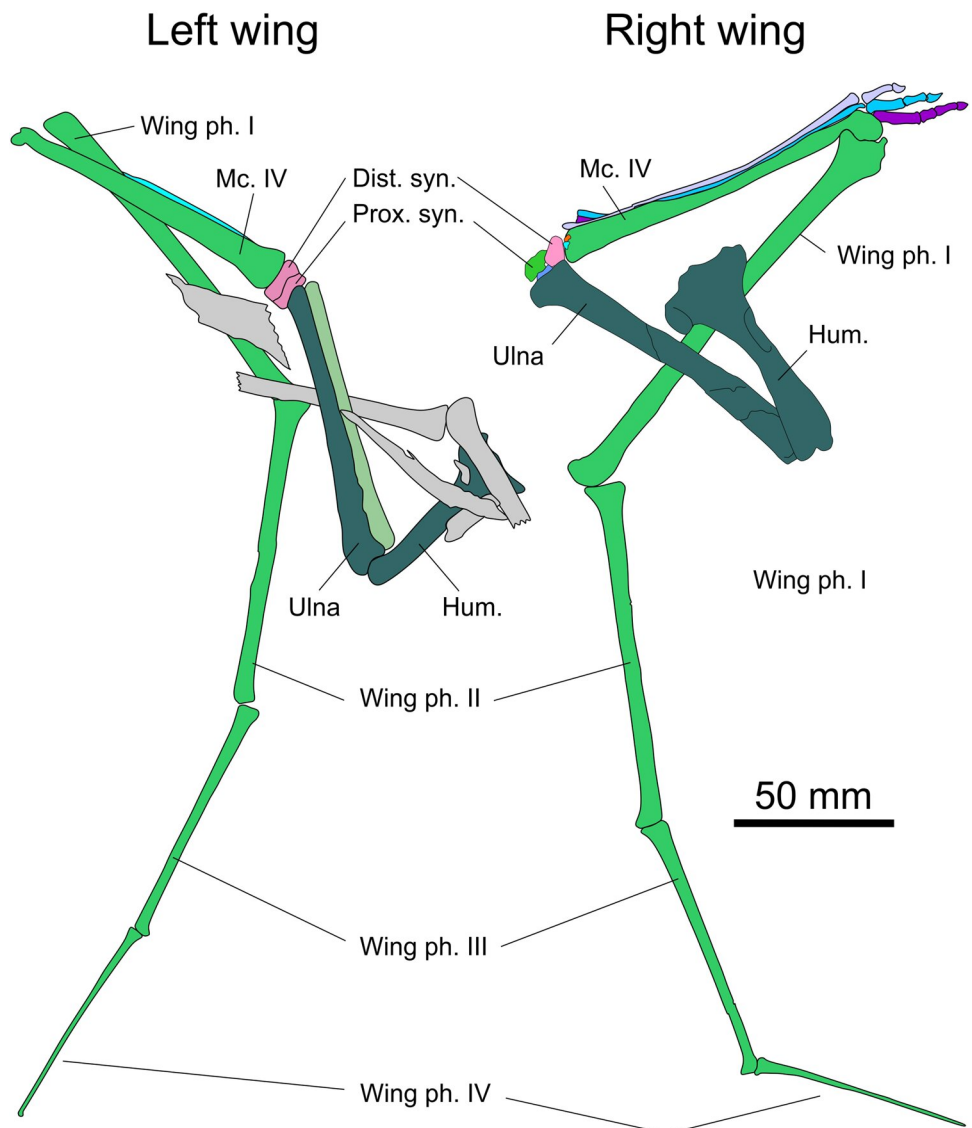
that in *Gnathosaurus*, *Ctenochasma roemeri*, *Pterodaustro* and *Pterodactylus* spp. but shorter than in *Cycnorhamphus* and *Ctenochasma elegans* (Bennett 2007) and likely *Beipiaopterus*, where phalanx 4 of the wing-finger is incomplete (Lü 2003). As for the limb bone ratios, *Balaeonognathus* is almost identical to *Cycnorhamphus* and closely resembles *Pterodaustro* (Fig. 14).

Diagnosis

Autapomorphies: The new specimen is distinguished as a new taxon on account of two conspicuous apomorphies: 1. terminal end of the jaws forming a triangular spatulate platform lacking teeth on its anterior border, 2. teeth long, slender and with a hook on the crown tip, 3. a unique combination of wing and hindlimb bone ratios typical of the Ctenochasmatidae.

Description

Skull

Skull. The skull (Figs. 2, 3, 4, 5, 6, 15) is complete and exposed in right lateral aspect. The periorbital bones are crushed, as are those of the occipitosquamosal area. The left mandibular ramus appears to lie in articulation with the left quadrate but the articulation itself is overlain by WP I and II of the right wing-finger. WP I also overlies the postorbital bar and the apex of the occiput (Figs. 2, 3, 5). The nasolacrimal part of the antorbital bar is slightly disarticulated, and

Fig. 11 *Balaenognathus maeuseri* gen. et sp. nov. (NKMB P2011-633): right hindlimb skeleton. **A** UV image; **B** interpretive drawing
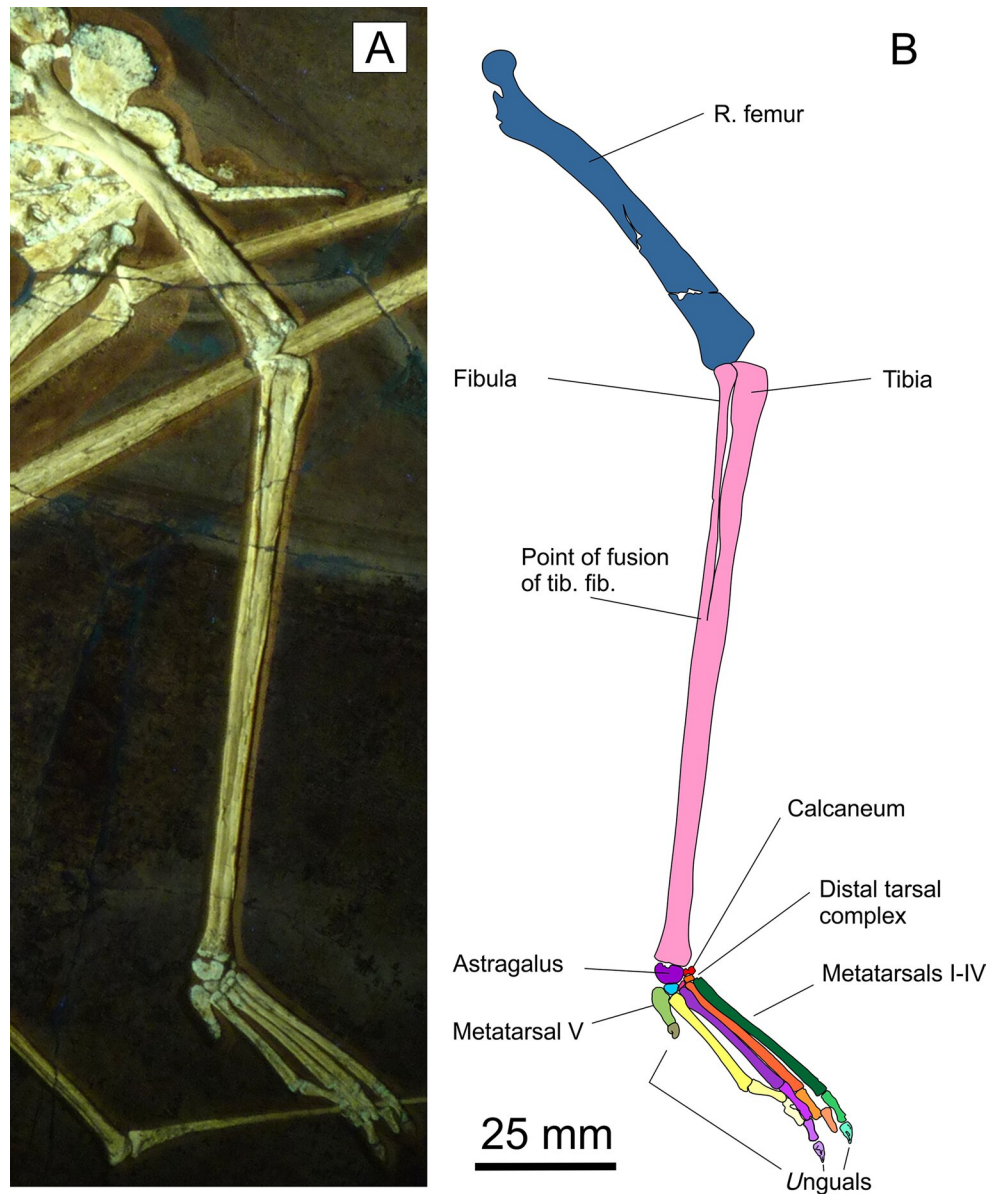
the posterior process of the premaxilla has become separated from the underlying part of the nasals.

The rostrum is about five times as long as the orbital part of the skull, measured from the anterior-most border of the orbit. Both the premaxillomaxillary and mandibular parts are curved dorsally, whereby the curvature of the premaxillomaxillary complex is slightly greater resulting in a gape at the anterior-most fifth of the jaws. The angle of the occlusal margins of the rostral curvature against that of the orbital part of the skull is estimated at approximately 30°. The precise angle cannot be assessed, because the anterior half of the mandible has rotated by about 80° around its long axis to the left now exposing the buccal face of the rostral expansion, whereas the posterior half of the mandible has more-or-less remained in place. Deformation of the

premaxillomaxillary complex comprises about 45° of clockwise rotation such that the left labial margin and the right buccal margins are exposed. The rostral expansion (henceforth called spatula) is partly obscured by the left tooth row and covered by matrix.

Premaxilla. The right premaxilla (Fig. 6) is visible in lateral aspect. It is likely that its anterior end forms the spatulate part of the upper jaw. The extent of the bone anteriorly cannot be reconstructed with certainty because of a fracture at the base of the rostral spatula, torsion of this element and the sediment infill. The premaxillae gradually converge posteriorly at an angle of about 5° and terminates as a narrow seam of bone forming the posterior concave roof of the skull. The premaxillomaxillary suture almost parallels

Fig. 12 *Balaenognathus maeuseri* gen. et sp. nov. (NKMB P2011-633): right pes skeleton. **A** UV image; **B** interpretive drawing. Ast., astragalus; Calc., calcaneum; Dist. tar., distal tarsal; Mt., metatarsal; Ph., phalanx; Pd., pedal; ung., ungual.; Tib., tibia
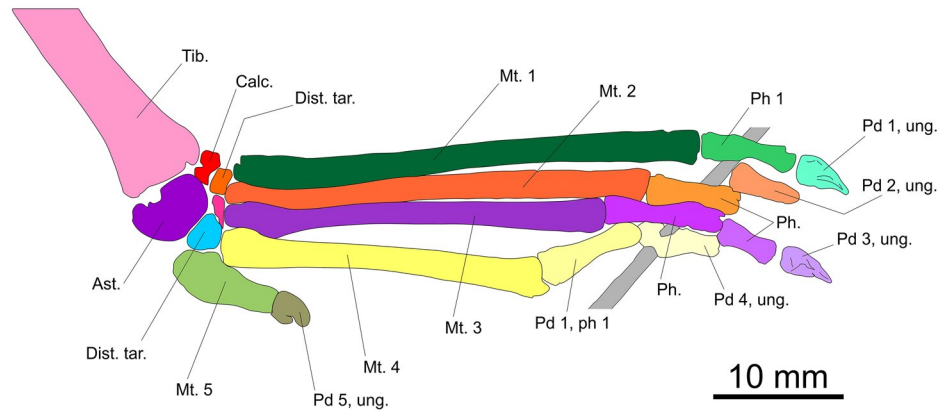
the dorsal margin of the rostrum. The dorsal margins of the premaxillae become convex level with the nasal process. From there the bone continues to taper and terminates with a pointed tip level with the middle of the dorsal margin of the orbit.

Maxilla. Only the right maxilla (Fig. 6) is exposed. The anterior end of the bone cannot be determined precisely because of the torsion of the rostral spatula. Likely, the bone forms a low vertical suture with the premaxilla at the base of the rostral spatula. The lateral wall of the maxilla gradually diverges posteriorly at an angle of about 3° thereby following the curvature of the rostrum. While its dorsal margin is concave, its dental margin is slightly convex in its anterior third. The convexity declines towards the middle part of the bone. In its posterior third the dental margin is almost straight. At the anterior margin of the nasoantorbital fenestra the maxilla bifurcates into two processes that taper posteriorly to a sharp point. The ventral one of these processes, the jugal process, forms the entire visible ventral margin of the nasoantorbital fenestra. Of the frontal process, only the base is visible forming the anterior corner of the nasoantorbital fenestra. The posterior termination of the frontal process is not visible.

The palatine process is visible along the entire extent of the maxilla. Anteriorly the process disappears below the left tooth row level with the assumed contact with the premaxilla. The palatine process exposes its full buccal face, which is deepest level with the anterior margin of the nasoantorbital fenestra. Despite the deformation due to compaction, the contralateral palatine process of the maxilla must have formed a deep keel that almost reached the ventral margins of the mandibular rami during maximum occlusion. The surface of the palatine process is slightly concave and marked by a longitudinal sulcus extending along the posterior sixth of the process.

Nasal. The right nasal (Fig. 6) is exposed in lateral aspect and has slightly rotated about its centre in a way that the anterior process has disarticulated from the premaxilla at an angle of about 5°. The right margin of the nasal has broken off. The T-shaped bone now underlies the posterior part of the left nasal. The contralateral nasals contacted the posterior sixth of the ventral margin of the premaxilla and formed the roof of the posterior fifth of the nasoantorbital fenestra. The posterior half of the left nasal forms a suture with the right frontal, but the shape of this suture cannot be assessed because the right margins of both bones are missing. Due
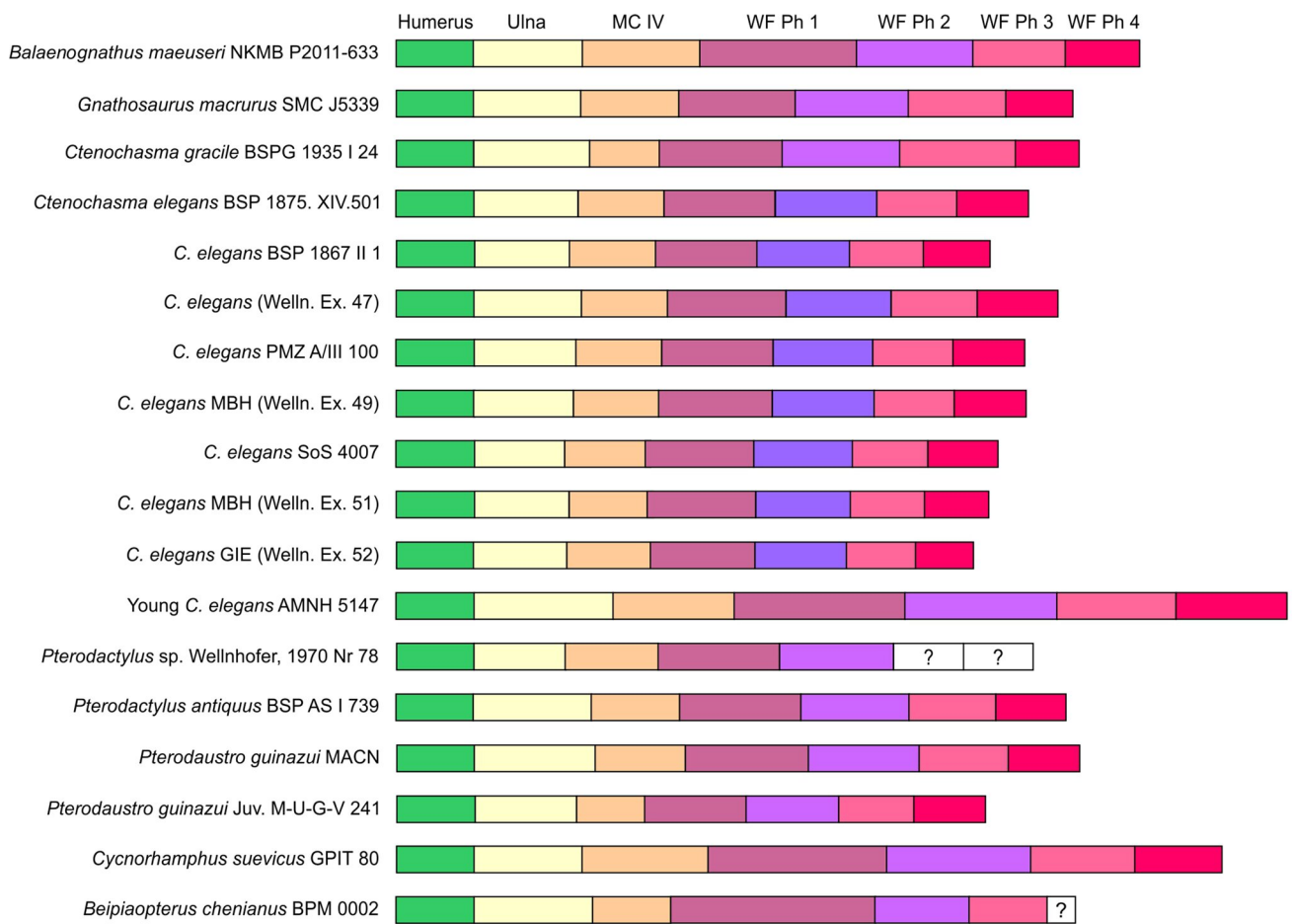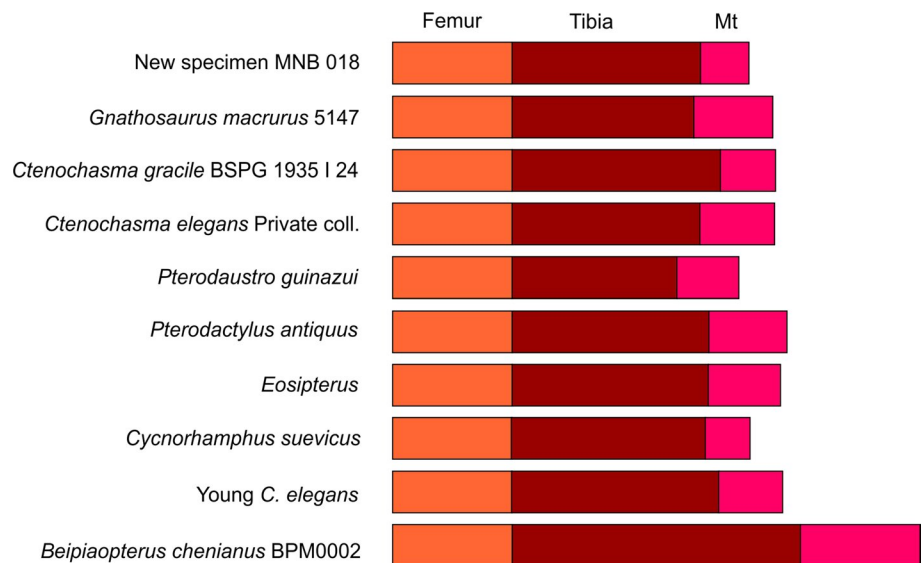
Fig. 13 *Balaenognathus maeuseri* gen. et sp. nov.: schematic diagram of the wing element ratios compared with other ctenochasmatid pterosaurs; *Gnathosaurus macrurus* (after Bennett 2013a), *Ctenochasma gracile* BSPG 1935 I 24 (after Wellnhofer 1970), all *Ctenochasma elegans*, after Bennett (2007), *Pterodaustro guinazui* (after Chinsamy et al. 2008), *Pterodactylus antiquus* (after Bennett 2013a), *Cycnorhamphus suevicus* (after Bennett 2013b), juvenile *Ctenochasma elegans* (from Wikimedia), *Beipiaopterus chenianus* BPM0002 after Lü (2003)

Fig. 14 *Balaenognathus maeuseri* gen. et sp. nov.: schematic diagram of the hind limb element ratios for compared with other ctenochasmatid pterosaurs; for references see Fig. 19
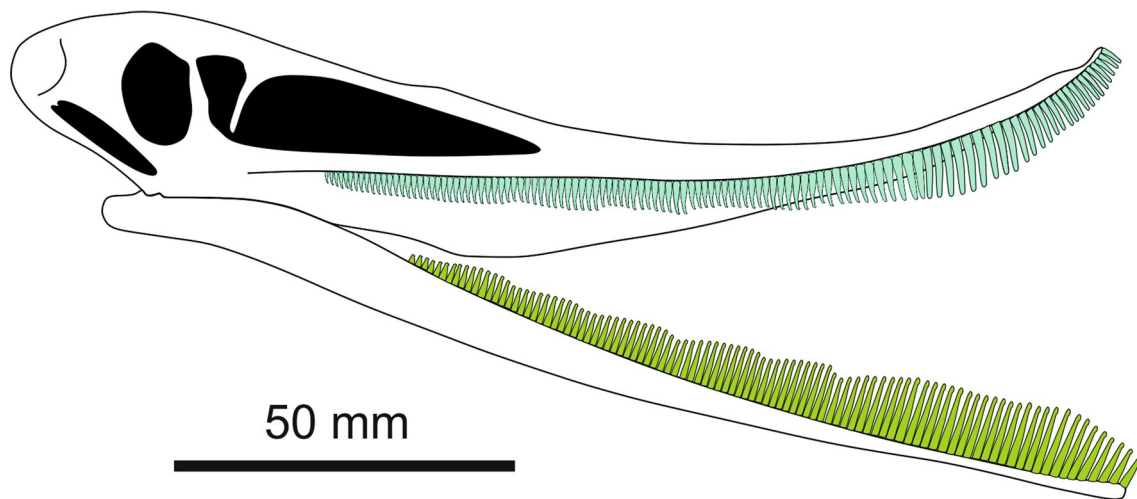
Fig. 15 *Balaenognathus maeuseri* gen. et sp. nov.: tentative line reconstruction of the skull

to multiple fracturing the exact shape of the nasal cannot be reliably reconstructed. The nasal process descends from about the middle of the ventral margin of nasal corpus as preserved and approaches the posterior end of the maxilla close to the supposed suture with the jugal. However, this area is overlain by the proximal end of WP II and is thus invisible. The anterior and posterior margins of the nasal process are slightly elevated. They unite level with the ventral half of the process to form a sulcus that widens dorsally around a vertical slit-like foramen. Only the anterior half of the body of the left nasal is preserved where the surface of the partially abraded median suture is exposed. This abrasion might have occurred during or after excavation when the slabs were moved.

Frontal. The lateral part of the right frontal (Fig. 6) is broken off such that the bone is exposed in longitudinal section. Likely the frontal overlaps the posterior third of the dorsal face of the nasal suggesting a squamate suture with the latter. Posteriorly the thickness of the frontal increases reaching a maximum at about the middle of the bone. Further posteriorly, the bone tapers again but apparently lacks its posterior end.

Lacrimal. The remaining of the corpus of the right lacrimal (Fig. 6) forms a suture with a concavity at the middle third of the ventral margin of the right nasal. The triangular descending processes of the contralateral lacrimals are preserved and contact the slightly concave posterior margin of the antorbital process of the jugals.

Jugal. The corpus and the postorbital process of the right jugal (Fig. 6) are obscured by the articulation of the right WP I and II as is the suture between the maxillary process

of the jugal and the maxilla. The antorbital process of the jugal raises posterodorsally at an angle of about 110° against the dental margin of the right maxilla. Immediately dorsal to the corpus of the right jugal there is a depression bordered by the elevated anterior and posterior margins of the antorbital process, which almost parallel each other until level with the dorsal end of this depression. A similar but much narrower depression is seen on the medial face of the antorbital process of the left jugal. From there, the slightly convex anterior and the slightly concave posterior margins of the antorbital process of the right jugal converge towards dorsally terminating in a sharp tip, which bears a shallow sulcus on both the lateral and medial faces. The descending process of both lacrimals lie in articulation with the posterior concavity of the tip of the antorbital jugular process. A small likely displaced fragment of the postorbital process of the jugal protrudes from below the right WP I.

Parietal. The only part of the parietal that appears to be preserved is the concave orbital margin (Fig. 6). The dorsolateral face of the parietal is impacted, and its orbital rim is slightly abraded such that the precise outline of the bone cannot be reconstructed. Due to the impaction, it remains unclear whether or not there was a parietal crest. However, it is evident that the dorsal face of the parietal was evenly convex. Due to fracturing nothing can be said about the anterior and posterior terminations of this bone.

Occipitosquamosal region. The dorsal third of this bone complex (Fig. 6) is overlain by the distal fourth of WP I. A compacted bone lamina suggests that the occipital was angled at about 100° against the dorsal face of the parietal. Thus, anatomical details of this area are not preserved. Due to the fragmentation of the occipitosquamosal bone complex

anatomical details of the participating bones cannot be determined.

Quadrate. The right quadrate (Fig. 6) lies in articulation with the occipitosquamosal complex and is seen in lateral aspect. The bone has rotated at 90° counter-clockwise such that the dorsal face of the articular condyle with the mandibular glenoid is exposed. Due to fragmentation, compression and compaction, the anatomy of the posterior articular end cannot be assessed. The anterior third is mostly covered by the retroarticular process of the right mandibular ramus. The bone is only broken transversely in is anterior third but is not compacted. The shaft of the quadrate reaches its narrowest diameter in its middle. The dorsal aspect of the anterior articular face of the right quadrate is visible ventral to the right retroarticular process. The articular head is saddle-shaped with a deep intercondylar sulcus, which is partly filled by matrix. The joint is about three times as wide as the narrowest point of the shaft. The entire bone is compressed in a way that nothing can be said about its original morphology.

The left quadrate is seen in medial aspect. Only the anterior two thirds of the shaft of the left quadrate can be identified. The dorsoventral extent of the articular condyle protrudes dorsally and is about twice as high as the narrowest diameter of the shaft. The posterior end of the bone has become incorporated with the occipitosquamosal bone mass.

Bone fragments inside the orbit. There are several bone fragments inside the orbit, five of which are platy and arranged in an arch, likely representing the posteroventral part of the sclerotic ring (Fig. 6). Probably two more fragments projecting vertically from the matrix, which are arranged nearly parallel to the anterodorsal margin of the orbit, may also belong to the sclerotic ring. The remaining fragments result from compaction of the interorbital septum.

Nasoantorbital fenestra. The nasoantorbital fenestra (Fig. 6) is elongate rounded triangular with the apex facing anteriorly. It covers about 50% of the antorbital part of the skull. The anterior margin of the nasoantorbital fenestra consists of a thin lamina extending from the sharply curved posterior margin of the base of the frontal process of the maxilla. The dorsal and ventral margins of the nasoantorbital fenestra diverge at an angle of about 20° in posterior direction until the fenestra reaches the height of the orbit. The dorsal margin includes an angle of about 80° with the posterior one. The ventral and posterior margins then must have included an angle of about 100°, but the posteroventral corner remains invisible because of the overlying WP II of the right wing.

Orbit. The orbit (Fig. 6) most likely had a rounded triangular outline. Despite it mostly being obscured the ventral margin was most likely sharply rounded as is suggested by the sharp curvature at the posterior base of the postorbital process of the right jugal. This suggests that the antorbital and postorbital processes of the jugal define an angle of ~ 120°. The anterior margin of the orbit is oriented nearly vertically. The dorsal margin of the orbit is not preserved but presumably angled at ~ 90° against the anterior margin with a sharp curve, which is anteriorly marked by the descending processes of the nasals. The shape of the posteroventral margin of the orbit is concealed below the distal third of the right WP I.

Temporal fenestrae. Both temporal fenestrae are completely obscured by the distal fourth of the right WP I (Fig. 6). Their outline thus remains unknown.

Mandible. The right mandibular ramus is visible in lateral aspect (Fig. 6). It is gently and regularly curved. Its anterior ninth forms the mandibular part of the rostral expansion with a slightly concave edentulous anterior margin, which is a little more than twice as wide as the narrowest transverse extension of the mandible at the base of the rostral expansion. The anterolateral corners of the rostral expansion are rounded and curve into the posterolateral margins of the spatula that anteriorly are almost straight. Towards posteriorly these margins become concave and finally merge with the dental margin of the dentaries.

While the rostral expansion lies almost parallel to the matrix surface the posterior end of the mandible is seen in an almost lateral aspect with both rami only slightly set-off against each other. Thus, the mandible has been twisted by about 80° clockwise around its long axis. That the symphysis remained in articulation posits two conclusions: (1) It must have been long, whereby its length cannot be determined. (2) It must have been rigid.

Surangular. The lateral aspect of the right surangular is only visible as a slender seam along the posterior sixth of the dorsal margin of the right mandibular ramus (Fig. 6). It is the only bone that is preserved as a distinct element within the mandible. No additional sutures nor the mandibular glenoid fossa can be detected, the latter being overlain by the posterodistal articular end of the right WP I.

The retroarticular process is only seen in the right mandibular ramus. The process is long, rectangular in outline and measures one tenth of the mandibular length. The right mandibular ramus reaches its greatest height immediately anterior to the likely place of the mandibular glenoid fossa below the posterodistal corner of the right WP I. The retroarticular process is one third lower. The lowest part of the mandible lies immediately posterior to the rostral spatula being half the height of the highest extension of the mandible.

Hyal apparatus. Both ceratohyals are rod-shaped, slightly curved and preserved in situ (Fig. 6). The posterior end of the right ceratohyal lies in articulation with the posteroventral corner of the retroarticular process, the left one likely, too. The anterior ends of the ceratohyals contact each other at an angle of about 15°. Under UV light the posterior fragment of the basihyal is visible, and in articulation with the ceratohyals.

Dentition. The upper jaws bear 130 slender and blunt teeth on either side (Figs. 6, 7, 8, 15, 16). About 16 of them appear to be premaxillary teeth but this is not certain because the premaxillomaxillary suture is not evident. However, it is likely aligned with a shallow impression shortly anterior to the base of the triangular extension of the upper jaw. The dentary tooth count is about 110 on either side. A precise number of teeth cannot be given because of the poor preservation of the teeth in the region of the rostral expansion. The difference in tooth count is due to the posteriorly shorter tooth row in the mandible. The minimum total tooth count is 480.

Most of the teeth sit in their respective alveoli (Fig. 6) with only a few being distorted or broken. Some are completely or partially preserved as external moulds. The apical end of the tooth crowns is blunt and extended into a nubbin or a hooklet, which is offset by a neck, and appears to be unique for the Pterosauria (Figs. 7, 16). The enamel appears to be thickened in the apical nubbins or hooklets (Fig. 16). In occlusion the teeth interdigitate, but due to their occlusal extensions full occlusion is not possible because of an interdental block. In the anterior third of the jaws, occlusion is impossible because of the diverging curvature of the upper jaw with respect to the mandible (Figs. 6, 15, 17). Here, the teeth are longest and thus still interdigitating despite the jaw divergence. The edentulous anterior margin of the rostral spatula left open an anteriorly facing rounded rectangular aperture.

The variable height of the teeth forms waves consisting of about 10 to 13 teeth counted from minimal height to maximal height (Fig. 8). In occlusion the maximum of such a tooth wave meets the minimum in the opposing jaws, warranting a regular interdigitation of the crown tips. These tooth waves may reflect an alternating pattern of tooth replacement, an assumption, which is supported by replacement teeth in the lowest areas of the waves.

The brownish enamel of the teeth is interrupted by cream-coloured rings that occasionally are correlated over several teeth (Fig. 16). These rings form bands that extend along the entire dentition and give the teeth a banded appearance. Likely this is an artefact of alteration of the tooth enamel and dentine at sites where incipient cracks have developed during compaction (Fig. 16). In all likelihood the banding reflects degrees of oxidation of organic matter within the enamel and dentine.

Vertebral column

Cervical series. Only the cervicals 4–6 are fully visible (Figs. 2, 3, 18). The rest of the cervical series is either covered by bones of the right wing or crushed beyond recognition anterior to the scapula and coracoid. The exposed vertebrae are crushed flat. Even the shape of the zygapophyses cannot be reconstructed with confidence. Cervical 5 is the longest of the series likely having been about four times longer than high. The neural spine is exceedingly low having only one fifth the height of the respective corpus and is restricted to its posterior fourth. The neural arches of cervicals 4 and 5 are as high as the corpus and separated from the latter by a sharp longitudinal ridge connecting crushed the pre- and postzygapophyses. In cervical 6 this ridge is massive with a blunt edge and the neural spine extends over posterior three fourths of the neural arch. From what is seen on the lateral face of the preserved anterior half of cervical 7, the massiveness of the lateral ridge appears to persist towards posteriorly.

Thoracolumbar series. Only the six posterior-most presacral vertebrae are fully visible (Figs. 2, 3, 5, 9) with the remaining seven overlain by the left radius/ulna such that only the middle part of their right transverse processes are exposed. All vertebrae are seen in dorsal aspect. Presacral 1 is slightly smaller than presacral 2, but otherwise these two vertebrae are morphologically identical. The transverse processes of both are subtriangular and extend between the pre- and postzygapophyses. The neural spine of presacral 1 expands beyond the caudal margin of its respective neural arch and fuses with that of sacral 1. The neural spine of presacral 2 has the same length as its neural arch.

While the width and length of the corpora of presacrals 3 to 6 equals that of presacral 2 as does the lateral expansion of the respective zygapophyses, the lateral expansion of the transverse processes and their width gradually increases by one fourth from one vertebra to the anteriorly following (Figs. 2, 3, 5, 9). The transverse processes of presacral 4 are inclined anteriorly at an angle of about 95° against the long axis of the corpus (Figs. 2, 3, 5). Their anterior and posterior margins are shallowly concave in a way that the lateral termini of the transverse processes form a set-off nubbin. Of presacral 6 only the right transverse process is complete. Its inclination towards anteriorly is the same as in presacral 5, but the concavity of its posterior margin is twice as deep as that of the anterior margin (Figs. 2, 3, 5). Despite being crushed, the neural spines of presacrals 5 and 6 appear to be as long as the respective
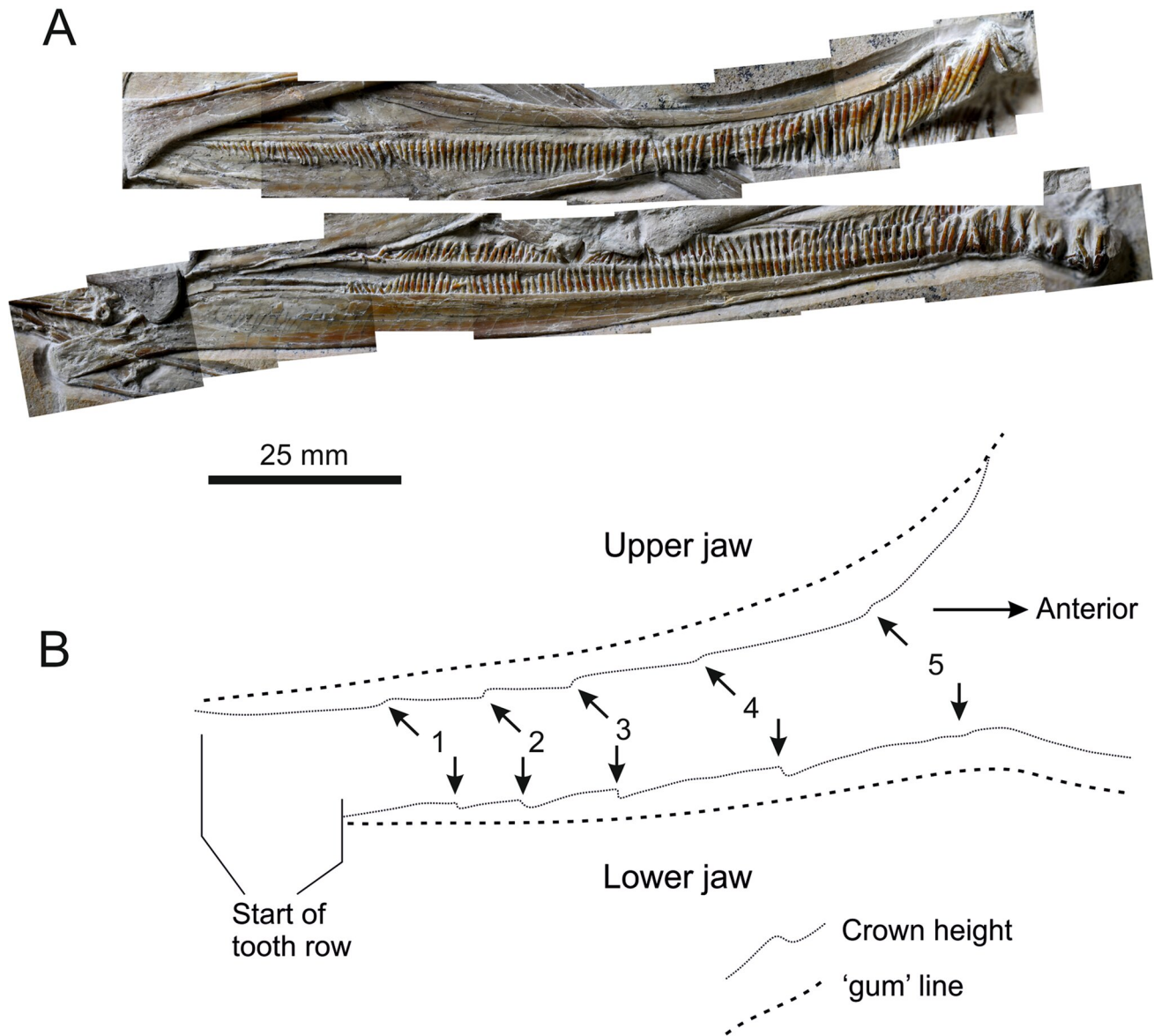
Fig. 16 *Balaenognathus maeuseri* gen. et sp. nov. (NKMB P2011-633): **A** photomontage of the entire dentition under normal light. **B** Line diagram of the dentition of the right side; finely dashed-line connects tooth crown apices, spaced dash line marls the jaw margins. Notice that there is a gradual increase in crown height towards anteriorly, followed by an abrupt reduction, likely representing a tooth replacement pattern. Arrows 1–5 identify the 'wave' peaks

neural arches. All thoracolumbar vertebrae anterior to presacral 3 bear ribs. Therefore, the lumbar region is formed by three vertebrae (Fig. 9).

Sacral vertebrae. The sacrum consists of at least five sacrals that are seen in dorsal aspect (Fig. 9). They are fused without a trace of a suture as are their neural spines. Because the posterior end of the sacrum is overlain by the right femur one, probably two more sacrals might exist. The anterior diameter of all visible sacrals is about 1/3 wider than the caudal one. The transverse processes extend along the entire lateral face of the neural arch and are inclined caudolaterally at an angle of about 70°. They are co-ossified with their respective corpora and the ilium. The lateral thirds of the sacrals are fused with each other leaving obliquely oval sacral foramina between them, which gradually decrease in size towards posteriorly. The long axis of these foramina is inclined at an angle of 60° in posterolateral direction against the median axis of the sacral corpora. The cranial margin of sacral 1 is sinusoidal with a shallow convexity in its basal third and a convexity, which is twice as deep in the anterolateral half, while the middle third is concave.
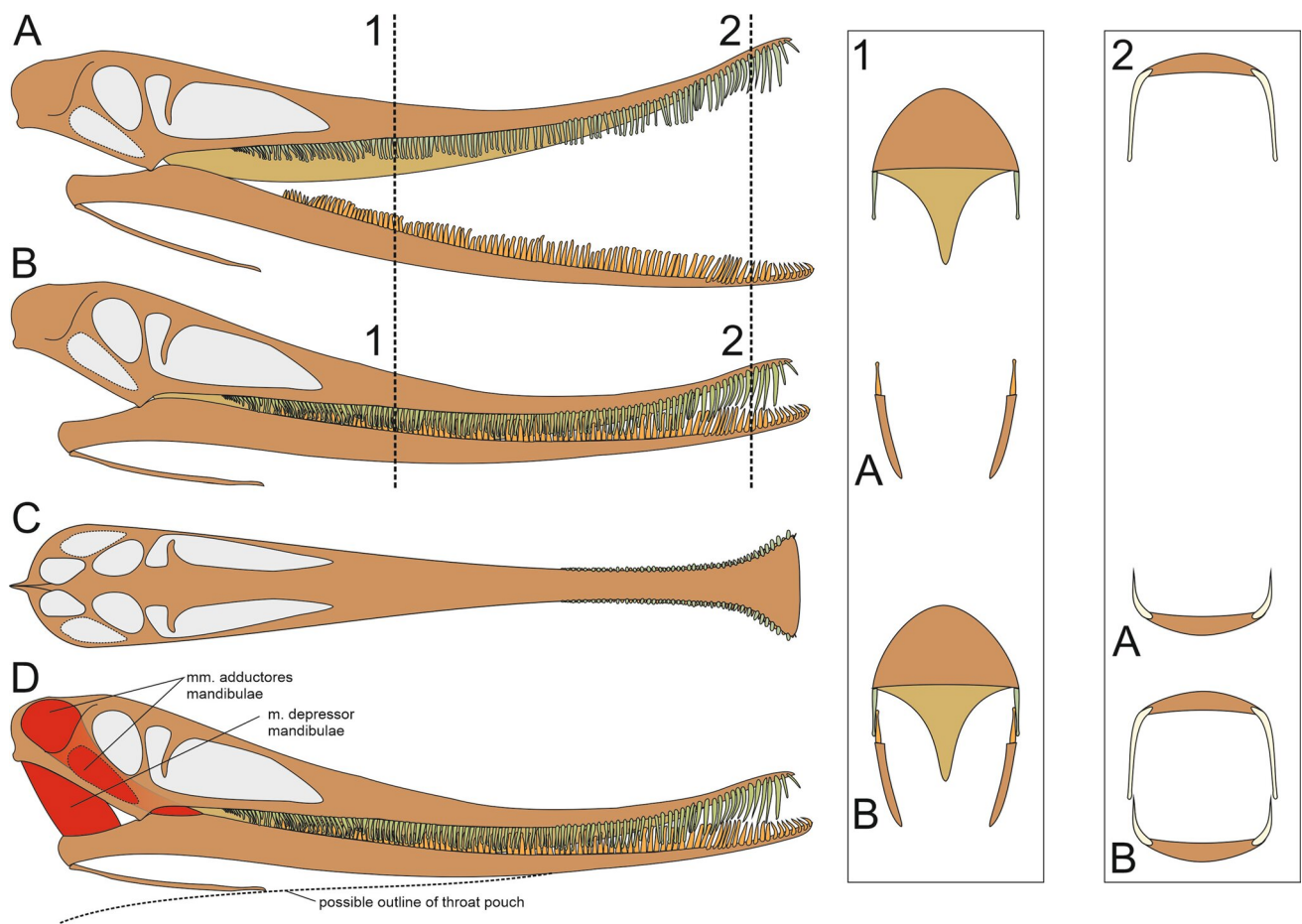
Fig. 17 *Balaenognathus maeuseri* gen. et sp. nov. interpretive drawings of the skull. **A** Maximum anatomical aperture of the rostrum; **B** rostrum in maximum anatomical occlusion; **C** dorsal aspect; notice the lack of a rostral tooth rosette; **D** reconstruction of the principal jaw adductors; notice the long retroarticular process. Musculature based loosely on Fastnacht (2005)

Caudal series. Twelve caudal vertebrae are visible (Fig. 9), however, the sacrocaudal transition is obscured by the overlying femur and the right ischium. Therefore, there is a possibility of one more caudal. The posterior half of the basal-most caudal vertebra is exposed in dorsal aspect. The second vertebra exposes its left face. All others are seen from ventrally. The dimensions of the first visible caudal cannot be assessed. The second visible vertebra is three times as long as it is high. Its corpus bears a shallow pleurocoel and a low rectangular neural spine reaching less than one fifth of the height of the corpus. The minimum diameter of the second visible caudal at its posterior end is one fourth its length and two thirds the diameter at its anterior end. The subsequent 10 caudals are almost truncated conical in outline and about one third longer than their maximum width. The minimum diameter is about two thirds of the maximum diameter, which is at the cranial circumference. The terminal two caudal vertebrae have a cranial articular circumference being half the vertebral length. The contralateral pleurocoels form a ventral keel that diverges towards the intervertebral articulations.

Ribs. Only the vertebral segments of the ribs are preserved (Figs. 2, 3, 5). All vertebrocostae are either still articulated or have only slightly moved laterally from their vertebral articulation but all of them have rotated posteriorly to varying degrees with respect to their vertebral articulation especially on the left side of the body, where the left humerus was squeezed into the thorax. On the right side 10 nicely preserved vertebral ribs are visible with the anterior-most three being twice as thick as the posteriorly following ones. Of the series the second visible vertebral rib is the longest. The length of the following vertebral ribs decreases with the posterior-most one being one fifth shorter than rib number 2. On the left side of the thorax, the 6 posterior-most ribs are visible, which equal their right counterparts in both shape and size.

Gastralia. The middle segments of five gastralia arcades (Figs. 2, 3, 5) are aligned with fragments of the lateral elements, which are scattered in the abdominal region. Their original arrangement and lateral extent in unknown.

Fig. 18 *Balaenognathus maeuseri* gen. et sp. nov. (NKMB P2011-633): cervical vertebrae. **A** UV image. **B** Interpretive line drawing; CV 1+2 are crushed, especially anteriorly, obscuring much detail; anterior portion of CV 7 largely obscured by MC IV and wrist elements; fragments likely coming from CV 8 and 9 are seen. Cor., right coracoid; cv, cervical vertebra; Mc. IV, right metacarpal IV; R. hum., right humerus; R. scap., right scapula; W. ph. 1, wing-finger phalanx 1; tv., thoracic vertebra
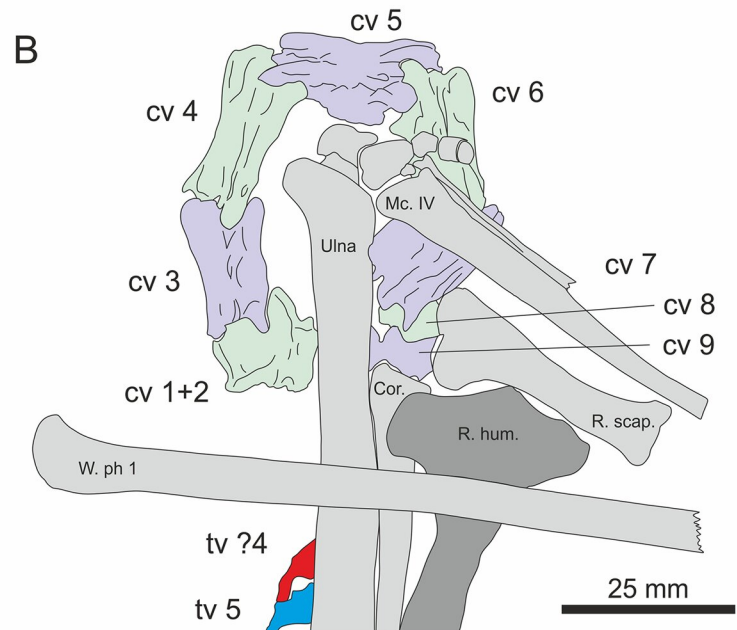

Sternum. The posterolateral two thirds of the concave and smooth internal face of the sternum are exposed (Figs. 2, 3, 5). The rest, including the cristospine, is obscured by bones of the right wing. The sternal plate is rounded pentagonal in outline with regularly rounded posterior terminus. The posterolateral margins converge at an angle of 90° and with the lateral margins include an angle of about 130°. The right margin is straight and devoid of any articulation facets with the sternocostal segments of the cranial three thoracic ribs. The left margin is not visible.

Prepubic bones. Only the right prepubic bone is preserved with its internal face exposed (Figs. 2, 3, 5). The medial fourth of the ala is overlain by the right femoral neck, a small part of in the lateral third of the anterior margin by vertebral rib 10. The prepubic bone has rotated by 90° medially from its original position, whereby the caudal terminus of the peduncle lies close to its original articulation facet. The peduncle anteriorly expands into an ala being approximately seven times as wide as the peduncle. The lateral and medial margins of the peduncle are sub-parallel and straight. The medial part of the ala of the right prepubic bone has a cranial margin, which is regularly convex. The caudal and medial margins of the ala are confluent with the margins of the peduncle, forming an even concavity. The angle between

Fig. 19 *Balaenognathus maeuseri* gen. et sp. nov. (NKMB P2011-633): detail of skeleton of left wrist. **A** UV image; **B** diagrammatic representation of wrist. Dent., dentary; Dist. syn. carp., distal syncarpal; Lat. Carp., preaxial carpal; Max., maxilla; Mc., metacarpal; Proc. syn. carp., proximal syncarpal; Rad., radius; Uln., ulna
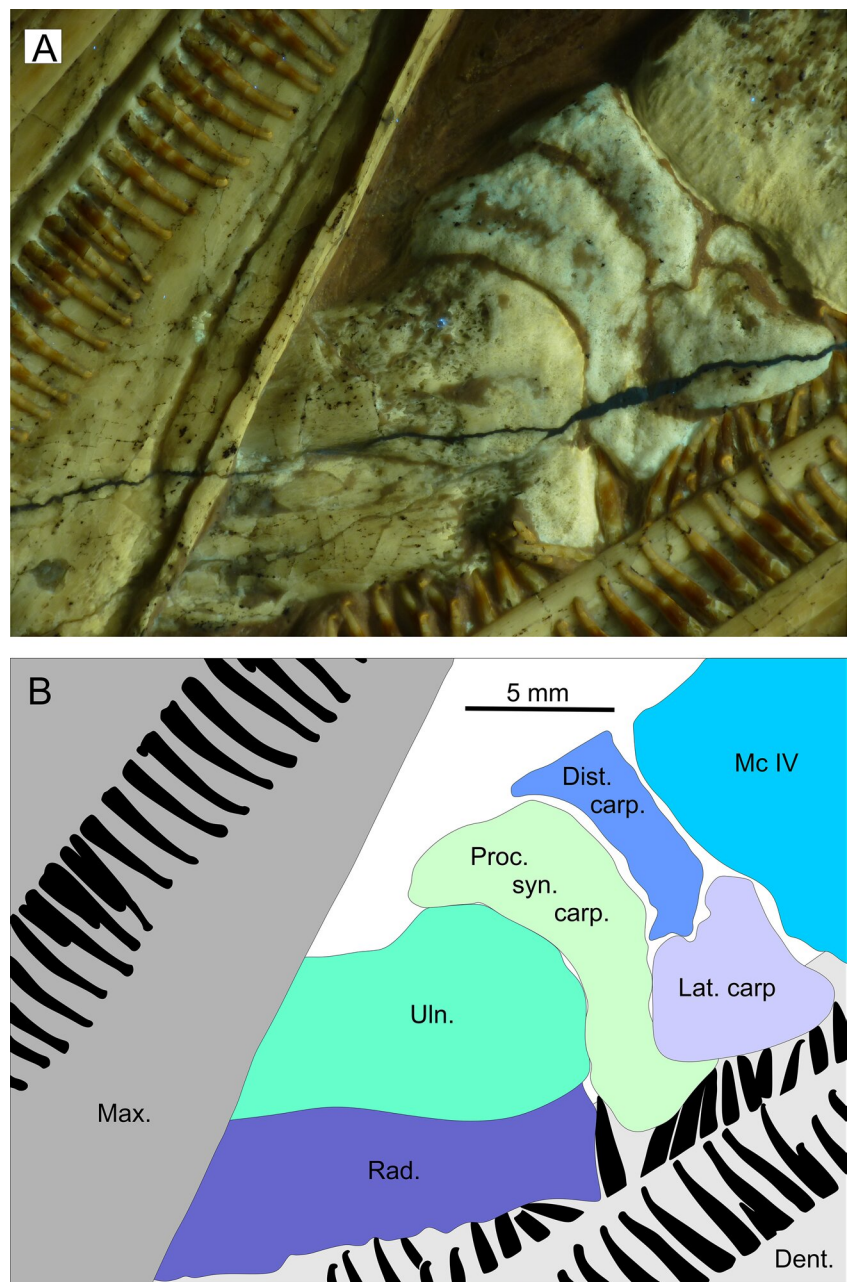

the anterior and posterior margin of the lateral part of the ala is about 30°.

Scapulocoracoid. The right scapula is disarticulated from the coracoid, of which only the glenoidal terminus is visible in dorsal aspect (Figs. 2, 3, 5). The scapula has rotated laterally and now exposes its medial face. The corpus makes about one third of the length of the scapula and at its glenoideal end is about twice as wide than at its dorsomedial margin. The posterior margin includes an angle of about 80° with the dorsomedial margin. The transition between the two is sharply rounded. The dorsomedial third of the posterior margin is shallowly concave followed by short convexity, which is again followed by a concavity that terminates immediately dorsal to the glenoid fossa. The anterior margin emerges from a sharp curvature at the anteromedial corner of the dorsomedial margin. From there it runs in a regular concavity in ventrolateral direction for about two thirds of the extent of the anterior margin. Then, the anterior margin becomes straight and terminates at the anterior edge of the scapulocoracoidal facet. This facet is convex and separated by a sulcus from the glenoid fossa, which has the same size as the scapulocoracoidal facet. The glenoid fossa is set-off posteriorly beyond the posterior margin of the scapula for about half its extension. The dorsomedial margin is shallowly sinusoidal with three small indentations,

Fig. 20 *Balaenognathus maeuseri* gen. et sp. nov. (NKMB P2011-633): detail of right wrist skeleton. **A** UV image; **B** interpretive drawing. Dist. sync., distal syncarpal; Lat. Carp., preaxial carpal; Mc., metacarpal; Rad. of prox. sync., radiale component of proximal syncarpal; Uk. of prox. sync., Ulnare of proximal syncarpal
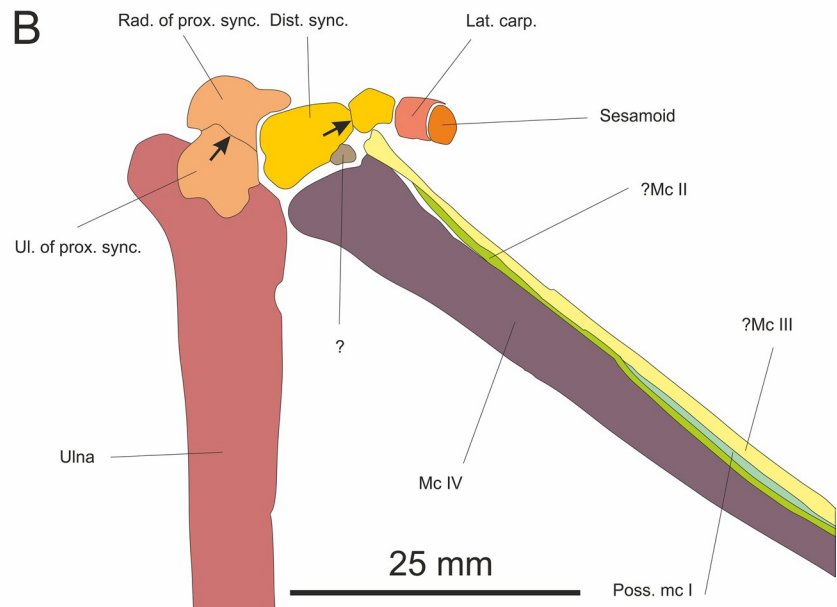
the anterior-most of them being the widest and deepest. The medial face of the scapular ala is slightly concave, whereas that of the corpus is convex. The articular face of the coracoid is rounded triangular as is the coracoidal part of the glenoid fossa, which opens posterolaterally. The glenoid fossa covers a little more than the caudal half of the dorsal face of the coracoid. Of the left scapula, only the dorsomedial and the dorsal fourth of the anterior margins are visible. Scapula and coracoid are unfused.

Wings

Both wing skeletons are complete and fully articulated (Figs. 2, 3, 5, 10, 19, 20). Both are flexed at the elbows, the right wing in almost total flexion (24° between humerus and forearm), the left at an angle of approximately 62°. The right wrist is flexed at an angle of approximately 59° between forearm and metacarpus, while the left is flexed at approximately 133°. In both wings, the flight finger has rotated tightly on the fourth metacarpal 'roller' joint (LW ~ 25°, RW ~ 57°) as though the wing fingers were folded over the body.

Humerus. The right humerus lies on its dorsal face with the deltopectoral crest facing craniolaterally with respect to the vertebral column (Figs. 2, 3, 5, 10). Its neck is crossed over by WP I, and its distal terminus is crushed. Of the left humerus, which is also lying on its ventral face, only the distal half is visible. The proximal half is overlain by WP I and the occipital area of the skull. In both humeri, the axis through the humeral head and the epicondyles include an angle of about 60°. On the right humerus the ventral epicondyle is exposed, on the left one the dorsal one. Both humeri are compacted. The following description is based on both humeri and only refers to the ventral face. The humeral head lies in line with the shaft and forms a convex protrusion that continues posteriorly into the proximal margin of a massive ulnar crest that extends over one fourth of the entire humeral length. The neck of the humerus continues straight into the shaft. The caudal margin of the ulnar crest forms a rounded blunt protuberance that is slightly warped ventrally. In anterior direction the humeral head is confluent with the concave proximal margin of the deltopectoral crest, the anteroproximal corner of which reaches the level of the humeral head. The anterior margin of the deltopectoral crest is regularly curved and continues into the distal margin of this crest, which merges with the shaft at about one fifth of the length of the humerus. Like the ulnar crest the deltopectoral crest is warped ventrally. Deltopectoral crest, humeral head and ulnar crest each form the proximal third of the humerus. The humeral neck is deeply concave ventrally in a way that the deltopectoral and the ulnar crests include an angle of about 120°. Distal to the neck, the humeral shaft is straight with a slightly concave posterior margin. Towards the epicondyles the shaft diverges and is one third thicker at its maximum diameter than at the mid-shaft. Both epicondyles are evenly rounded. The dorsal one, which is one third larger than the ventral one, protrudes in anterodorsal direction. The trochlea is about half the size of the capitulum and partially covered by the left ulna. A long-oval muscle scar is visible in the distal fourth of the left humerus in middle of the ventral face proximal to the ventral epicondyle likely the attachment pit for the m. brachioradialis.

Ulna. Both ulnae are preserved in articulation with humerus, carpus and radius of either wing (Figs. 2, 3, 5, 10). The right ulna is seen from ventrally, the left one from posterodorsally. The following description is based on both ulnae. The diameter of the proximal articular face is twice as wide as that of the distal one. The proximal articular surface shows a trochlear notch, which is divided by a tiny anconeal ridge into a dorsal and a ventral cotyle. The ventral cotyle is about twice as broad as the dorsal one. The anterodorsally pointing glenoidal tuberosity has one third the width of the entire joint and barely protrudes beyond the proximal articular face of the ulna. The dorsal cotyle terminates in a low and blunt anteriorly facing coronoid process that distally immediately merges with the anterior face of the ulnar shaft. The ulnar head converges into the shaft with a curvature angle of about 175° while the anterodorsal face of the ulna is slightly convex the caudal one is slightly concave. The smallest diameter of the shaft is in the middle, where it comprises a little more than half the diameter of the head. Towards distally, the shaft slightly curves posteriorly. At the articulation with the carpus (Figs. 19, 20), the ulna diverges again and, at its distal extremity, is as wide as the ulnar head. In lateral aspect, as is seen in the left ulna, the condyle of the distal articular face is sub-circular and bears a blunt ridge that merges with the distal margin of the dorsal condyle. The distoventral styloid process is low and blunt and overlaps the cranial corner of the radius. Because both ulnae are crushed, further anatomical details cannot be described due to compaction.

Radius. Both radii are in articulation with their respective ulnae and are thus only partially visible (Figs. 2, 3, 5, 10). The right radius is mostly obscured by the right ulna with only its anterior margin visible and revealing nothing noteworthy. In contrast, the left radius is fully exposed and seen from anterodorsally. The head of the radius articulates with the anteroventral face of the dorsal glenoidal tuberosity and contacts the dorsal condyle of the humerus with an ovoid articular head, which is slightly set-off in anterior direction. Immediately distal to the articular surface there is a shallow depression in the anterior face of the bone. From there, the shaft diameter of the radius remains constant with the anterior and posterior margins running parallel to each other distally for two third of the bone and they diverge slightly towards the distal articular head which lies in contact with the distal articular face of the left ulna. No further structural details are seen on the bone because of the compaction.

Carpus. The proximal and distal syncarpals are preserved in articulation in the left wing only and are seen in dorsal view (Figs. 19, 20). The right carpus has been slightly displaced, and the four carpals now lie in a single row along the proximal articulation face of the wing-finger metacarpus. In dorsal view the ulnare is semi-lunate with a concave proximal articular margin that matches the distal 'roller' of the ulna. The anterior and posterior margins are only slightly convex and have one third the length of the proximal one. The distal margin of the ulnare is marked by a strong convexity in the middle that becomes shallower anteriorly and posteriorly.

The radiale is half the size of the ulnare. Its distal margin bears two facets, of which the posterior one is twice as large as the anterior one. The posterior articular face is shallowly concave and accommodates the distal apex of the distal ulnar articulation. The anterior one is slightly convex. Both include an angle of about 120°. The caudal margin of the radiale is half as long as the posterior proximal articular

face, slightly concave and contacting the anterior margin of the ulnare. The angle between the posterior margin and the posterior proximal facet is about 95°. The cranial margin is a little longer than the anterior proximal facet and bears a concavity in the middle. The anterior margin of the radiale forms a right angle with the anterior proximal facet. The distal articular facet is regularly concave and lies in articulation with the anteroproximal articular process of the anterior distal carpal. This process forms the proximal margin of the anterior distal carpal. It merges with the anterior margin together forming a semicircular structure. The distal margin of the bone is slightly convex and lies in articulation with the anterior proximal articular face of the wing-finger metacarpal. The posterior fifth of the distal margin of the anterior distal carpal is angled against the main part of this margin at about 160°.

The posterior margin of the anterior distal carpal is concave and measures two thirds the length of the distal margin and contacts the anterior margin of the posterior distal carpal, which is convex and proximally terminates in a small process that wraps the anterior margin of the ulnare with its tip contacting the posterodistal corner of the radiale.

The proximal margin of the posterior distal carpal is concave and perfectly fits the anterior two thirds of the distal margin of the ulnare. The posterior margin of the posterior distal carpal is sinusoid and about half as long as the proximal margin. The caudal margin of the bone is almost straight ending in a posterodistally facing tiny process. The concavity matches the posterior articular face of the wing-finger metacarpal. The four bones, of the right carpus cannot be referred to distinct carpals as it is unclear which faces are exposed.

Pteroids. Despite both wrists being in an excellent state of preservation and articulation, both pteroids are missing. While it is possible that these elements are concealed underneath forearm elements, they are not visible on the X-ray (Fig. 4). It appears plausible that they were unossified given the excellent general state of preservation. We know of no pterosaur in which the pteroids are absent.

Metacarpus. The right wing-finger metacarpal is exposed in dorsal view the left one in anterior view (Figs. 2, 3, 5, 10). The distal articulation is only seen in the right wing-finger metacarpal. In the left, this part of the bone is cut by the border of the original slab. The metacarpals of digits I-III lie in an in situ position in the right wing. In the left wing, only one single metacarpal is visible ventral to the wing-finger metacarpal.

The anterior margin of the carpometacarpal articulation of the left wing-finger metacarpal shows two low convexities of equal size separated by a narrow interarticular indentation. From the proximal articular face towards the distal end, the bone converges gradually until its distal seventh. Then it converges more rapidly towards the distal articular joint at the base of which the bone reaches its smallest diameter, which is one fourth of that of the proximal articular face seen anteriorly. The neck of the distal 'roller' joint is slightly curved ventrally at an angle of about 170° against the long axis of the shaft. The anterior face of the wing-finger metacarpal is shallowly concave. The concavity begins immediately distal to the proximal articular face and deepens distally until the base of the ventrally bent neck of the distal 'roller' articulation. There it terminates in a marked depression that may contain a pneumatic foramen. Dorsally and ventrally the concavity is bordered by a ridge that gradually sharpens towards the distal end of the concavity. Of the distal 'roller' joint of the left wing-finger metacarpal only the dorsal condyle is visible, which is oriented with the long axis of the shaft.

The dorsal aspect of the right wing-finger metacarpal reveals that the diameter of the bone at its proximal articulation face is about twice as high as it is wide. At about mid-shaft the diameter becomes circular with the above-mentioned anterior concavity. In dorsal aspect, the margin of the proximal articular face is shallowly convex and inclined against the long axis of the shaft at about 75° in anterior direction. The proximal articular head is set-off from the shaft by shallow concavities on the anterior and posterior face of the bone. These concavities have the same length as proximal articular face. On the posterior face the concavity is followed by a low ridge of the same length as the concavity. Distal to that ridge the wing-finger metacarpal converges towards distally until the base of the distal 'roller' joint there the diameter is about half of the diameter of the proximal articular face in dorsal aspect. The shaft of the wing-finger metacarpal is gently curved anteriorly at an angle of about 177° until the neck of the distal 'roller', where the curvature increases to about 165°, before it curves caudally at the base of the distal 'roller' joint. The dorsal condyle of the distal 'roller' joint is semicircular, shows a groove that extends parallel to its apex and anterior margin. The dorsal face of the bone is slightly compacted.

Metacarpals of digits I–III. Only the metacarpal of digit I extends to the carpus. The metacarpal of digit II extends proximally for about four fifth of the wing-finger metacarpal and metacarpal III for one third (Figs. 2, 3, 5, 10). The maximum diameter of these three metacarpals at their distal terminus is about one third of the smallest diameter of the wing-finger metacarpal at the constriction behind the 'roller' joint. The proximal end of metacarpal I is hidden below one of the carpals. The proximal end of the remaining two are pointed. The distal articular ends of these rod-like, cylindrical bones are rounded. On the left wing, only the middle half of metacarpal I is visible.

Phalanges of digits I–III. Only the right manus is preserved (Figs. 2, 3, 5, 10). All phalanges of the three free digits are preserved and fully articulated and are seen in dorsal aspect. The phalanges of the three small digits are slightly compacted, especially at their articular heads. The planes of the articular surfaces of the phalanges of digit III are at right angle to the long axis of their shafts. That of digit II includes an angle of about 65° with the long axis of the shafts and runs in posteropalmar direction.

Digit I. The proximal joint of the basal phalanx of digit I has two third the width of the distal metacarpal condyle and is convex. The proximal articular head is twice as wide as the distal one. The length of the shaft is five times its maximum width. The bone is slightly sigmoidal with the distal third curving posteriorly.

Digit II. The basal phalanx of digit II is one fourth longer and wider than that of digit I. The morphology of the proximal articular head coincides with that of digit I, and the shaft has its minimum diameter in the middle. The diameter of the distal articular head is a little smaller than that of the proximal one. The basal phalanx of digit III differs from that of digit II in being one third longer and one fourth wider. Furthermore, it shows a sigmoidal curvature, whereby the proximal third is bent posteriorly the distal two thirds palmarly. The anterior and posterior margins run parallel to each other. The overall shape of the proximal articular head coincides with those of digits I and II. The distal one is shallowly convex.

The second phalanx of the second digit is one third shorter and thinner than the basal phalanx of digit II. The articular heads are evenly rounded, whereby the proximal one is one third wider than the distal one. The apex of the proximal articular head raises in the palmar third of the articular face resulting in an oblique articular suture (see above). Distally the palmar margin of the ventral condyle is just visible indicating that the distal joint of the second phalanx is a saddle joint.

Digit III. The basal phalanx of digit III is the largest of the free fingers being one third longer and thicker than the basal phalanx of digit II. The proximal articular head of the phalanx is overlain by the proximal articular head of the basal phalanx of digit II and the 'roller' joint of the wing-finger metacarpal. The bone is cylindrical with almost parallel sides. Its distal fifth is slightly curved palmarly. The distal articular head of the basal phalanx of digit III is slightly convex and set-off from the shaft by a shallow circumference but the articular face has the same diameter as the shaft. The second phalanx of digit III has one third of the length of the basal phalanx. In dorsal aspect, the proximal articular face of the second phalanx is concave in the middle two thirds and is as wide as the distal articular hear of the basal phalanx. Towards the distal end, the second phalanx of digit III converges symmetrically. The distal articular head is evenly convex and measures one third the width of the proximal one. The penultimate phalanx of digit III is one third longer than the second one and one third narrower at the proximal articular face, which is concave. From there the anterior and posterior margins of the phalanx converge for one third of the length of the bone where a mid-shaft constriction is seen. From the narrowest point of this constriction in the middle of the phalanx the margins diverge again until the distal articular head.

Ungual phalanges. All three ungual phalanges are of similar shape, but that of digit III is one third shorter and slenderer, with a length/width ratio of 1:4. The unguals of digits I and II have a length/width ratio of 1:2. The adductor tubercles in all unguals are minute and rounded and form the palmar extension of the articular cotyle. Between the adductor tubercle and the apex, the palmar margins of the ungual phalanges are regularly concave. The ungual of digit I has one third of the length of the penultimate phalanx. The unguals of digits II and III are as long as the respective penultimate phalanges.

Wing-finger (Figs. 2, 3, 5, 10; for a comparative wing bone ratios see Fig. 13).

Wing-finger phalanx I. WP I is one fourth longer than the respective wing-finger metacarpal and preserved in both wings, whereby the proximal articular head of the left one is missing. The proximal articulation of the basal wing-finger phalanx is the trochlea of which only the sub-circular dorsal margin is exposed. The posterior articular process is hook-shaped, and its proximal margin measures one third of the trochlea with which it is confluent. From its posterior terminus the process bulges a little and then curves anteriorly to merge with the shaft. The cranial articulation is twice the size of the caudal one and is semicircular in outline with its rounded anterior margin confluent with the shaft and level with the posterior articular process. The extensor tendon process sits on the proximal extremity of the anterior articular process. It is a semi-lunate structure in dorsal view with a concave distal articular face. A spine arises from the proximal apex of the extensor tendon process. The extensor tendon process is not co-ossified with the proximal margin of the anterior articular process and forms one fourth of the dorsal trochlear margin. The cranial and caudal margins of the proximal articular head almost symmetrically converge towards distally. In about the middle, the shaft reaches its minimum diameter, which is half of the proximal one including all processes. From there, the shaft gradually diverges again to the distal articulation, whereby the cranial margin

is slightly concave until the neck of the distal articular head, where it curved posteriorly into the distal articular head. The caudal margin of the shaft is slightly concave. This concavity increases distally to form the neck of the distal articular head. The distal articulation expands posteriorly by one third of with respect to the diameter of the neck. The distal articular head is evenly rounded in dorsal aspect and stands at a right angle to the long axis of the shaft.

Wing-finger phalanx II. WP II is best seen on the right wing, where it is fully exposed (Figs. 2, 3, 4, 5, 10). The dorsal margin of the proximal articular head of the WP II is straight and posteriorly terminates in a sharp process. A blunt ridge marks the anterior margin of the proximal articulation. Distal to this crest the anterior margin of the shaft is straight and slightly curves posteriorly at the neck of the distal condyle. In the neck region of the proximal articular head, the posterior margin is concave and from there gradually becomes straight in its proximal fifth and then parallels the anterior margin until the neck of the distal articular head, where it curves posteriorly. The minimum diameter of the shaft is in the middle of the shaft, where it is about two thirds of the diameter at the proximal articulation. The distal articulation is two thirds the size of the proximal one.

Wing-finger phalanx III. WP III of both wings are well exposed. Its shape is identical with that of the WP II but is one fifth smaller, and the posterior margin of the shaft is slightly concave (Figs. 2, 3, 4, 5, 10). All ratios are identical to those of WP II.

Wing-finger phalanx IV. WP IV is three fourths the length of WP III. In both wings, the shaft is straight (Fig. 10). The dorsal margin of its proximal articulation is slightly concave. The posterior margin of the bone in the left wing in the proximal fifth converges in a straight line towards the shaft. Then, distal to a shallow concavity the anterior and posterior margins converge to the distal terminus of the bone, which is only preserved on the right wing. Here, the wing tip is blunt and has one fifth the diameter of the proximal joint. In the fourth wing-finger phalanx of the right wing the caudal margin along the proximal fifth of the bone is concave and not straight as it is in the left wing.

Pelvic girdle

The pelvis as a whole has been pressed over its left half such that both iliosacral joints acted as a hinge during the left hand side movement (Figs. 2, 3, 4, 5, 9). The left side of the pelvis therefore is mostly obscured by the sacrum and the right femur that overlies the postacetabular part of the ilium. The acetabulum and part of the left ilium is seen in dorsal aspect. The acetabulum bears a dorsal ridge that reinforces its entire roof. Posterior to the acetabulum a deep concavity is visible suggesting a narrow base of the postacetabular process, which is confirmed on the right ilium, where this process has two third the diameter of the preacetabular process. The rounded posterior fourth of the left ischium is seen medially. The acetabular region of the right half of the pelvis is overlain by the right femur as is the peduncle of the pubis and the base of the ischium. The preacetabular process is parallel-sided and slightly curved medially. The external face of the ala of the right pubis is visible adjacent to the head of the right femur. The anterior margin of the pubis is very slightly convex and sharply turns posteriorly into the ventromedial margin, which bears two convexities separated by a shallow concavity. The posterior convexity is one fourth shorter than the anterior one and strongly curves dorsolaterally to form a hook-like process with a deep dorsal concavity that merges with the posterior margin of the bone. The degree of convergence between the anterior and posterior margins as preserved suggests a narrow pubic peduncle. The hook-shaped pubic process contacts the anterior margin of the ischium thereby framing a large oval obturator foramen. The ventromedial margin of the ischium is rounded with a narrower curvature in its posterior third. The anteroventral margin of the bone is strongly curved and merges with the anterior margin, which is slightly concave towards is base. The posterior margin is concave. The base of the ischium is about one third narrower than the maximum extent of the ala.

Hind limbs

Both hind limbs are complete and in articulation with the acetabula or approximately so (Figs. 1, Figs. 2, 3, 4, 5, 18, 20: for the comparative limb bone ratio see Fig. 14).

Femur. The left femur is seen in dorsal aspect and is preserved in full articulation with the acetabulum, but it is badly crushed (Figs. 2, 3, 4, 5, 11, 12). The shaft of the femur curves gently laterally. The right femur, which has rotated out of the acetabulum in a dorsomedial direction, is seen in dorsolateral view. The flat and in lateral view oval femoral head is set-off by a neck, which is strongly curved posterolaterally. It measures one sixth of the entire femur length. The blunt fourth trochanter then rises from the posterolateral margin of the femur marking the transition between femoral neck and shaft. The curvature of the femoral neck continues until the middle of the shaft thereby gradually becoming shallower. Distally to the end of the curvature the shaft is straight and slightly diverges towards the knee joint. The epicondylar relief is so weak that only the lateral condyle is visible as a low convexity arising from the distal face of the bone. The lateral epicondyle is medially set-off by a ventrolateral concavity, where the lateral and medial

margins diverge. The medial epicondyle is flat in both distal and medial directions. The distal articular face of the femur is about one third wider than the narrowest part of the shaft.

Tibia. Both tibiae are seen in lateral view (Figs. 2, 3, 4, 5, 11, 12). The tibia is about twice as long as the femur. The tibial head is three times as wide as the narrowest part of the shaft, a constriction proximally adjacent to the distal joint. The articular surface of the tibial head is at a right angle to the long axis of the shaft. From the circumference of the proximal articulation surface the tibia converges distally, whereby the posterior margin immediately distal to the articular face is slightly concave and the anterior one convex forming a low cnemial ridge extending over the proximal one tenth of the shaft. The distal two thirds of the lateral face of the cnemial crest bears an elongate oval depression. The distal joint is half as wide as the proximal one. An incision separates the distal articular face in two very flat condyles of almost equal size with the posterior one being a little smaller. This structure is not visible on the left tibia, neither is there a cnemial crest or a concavity distal to the proximal articular face.

Fibula. Both fibulae are exposed from their right sides (Figs. 2, 3, 4, 5, 11, 12), and lie in articulation with the respective tibiae. The fibula is about 40% of the length of the tibia. The fibular head is triangular in lateral view with a neck that measures about one eighth of the bone. Distal to the neck there is an expansion which is about as long as the fibular neck. From the end of this bulge, the fibula tapers to its distal end, which is pointed.

Tarsus. The right tarsus is preserved in dorsolateral the left one in lateral view (Figs. 2, 3, 4, 5, 11, 12). In the right tarsus astragalus and calcaneum as well as three distal metatarsals are visible in anatomical articulation. In the left pes, the astragalus and two distal tarsals are visible.

The calcaneum lies medial to the astragalus and has a rounded irregularly pentagonal outline in lateral view. The straight proximal margin is approximately three-quarters the length of the distal articular face of the tibia. The anterior margin forms a right angle to the proximal margin and is also straight. The distal margin includes 90° with the anterior one and is slightly convex with a shallow concavity in the middle. The posterior margin of the calcaneum is angled against the distal one at about 100° and extends into a small blunt process at two thirds of the posterior margin in proximal direction. The margins of this process include an angle of about 120°. The lateral surface of the astragalus shows a central depression and the corners are a little elevated. At least the lateral half of the astragalus is covered by the calcaneum. The visible medial part bears a sulcus forming a sharp longitudinal depression.

The distal tarsals are here numbered from medial to lateral as 1, 2 and 3. Distal carpal 1 is situated between the proximal articulation heads of metatarsals I and II and inside the sulcus on the astragalus. The bone is ovoid and is one sixth the size of the calcaneum. Laterally adjacent lies distal tarsal 2, which is one third smaller than distal tarsal 1 but of the same shape. The long axes of both are oriented transversely. Distal tarsal 3 is twice as large as distal tarsal 1 and rounded semicircular in outline. The flat face contacts the distal margin of the calcaneum, the rounded face reaches between metatarsals III and IV and laterally articulates with metatarsal V.

Metatarsus. The metatarsals are all nearly fully exposed and seen in dorsal view (Figs. 2, 3, 4, 5, 11, 12). The angle between metatarsal I and II is 2° and that between II and III is just 1°. Metatarsals II and IV diverge by about 5° while metatarsals IV and V diverge by approximately 6°. The metatarsals of the left pes overly each other obscuring most osteological features. Only the heads of metatarsals I to IV overlay each other a little, but the shape of the head is visible and alike in all these four metatarsals. It is an ovoid joint with a semicircular articular face. The distal articular heads form a horizontal 'roller' joint of the same transverse diameter as the proximal articular heads in metatarsals II, III and IV. In metatarsal I the proximal articular head is about one third bigger. The shafts are slightly curved laterally with convex lateral margins. The minimum thickness of the metatarsals I to IV is about mid-shaft.

Metatarsal I is the longest of the series measuring one third of the tibia length. Metatarsal II is one ninth shorter than the first, metatarsal III lacks one seventh of the length of metatarsal II and metatarsal IV has one fifth the length of metatarsal III. The distal ends of metatarsals I to IV terminate in a straight line. The fifth metatarsal is rounded with a subtriangular outline and is one fourth the length of metatarsal IV. Its proximal end is rounded and one third wider than the shafts of the other metatarsals. Adjacent to the distal end of the bone the medial margin has a concave articulation facet for distal tarsal 3 with its widest point in the proximal third.

Phalanges. The pedal phalangeal formula is 2, 3, 3, 4, 1 (Fig. 12). The ungual of digit II as well as the penultimate phalanx and the ungual of the right pes are missing. The penultimate phalanx of digit II is displaced medially from its original articulation. The basal phalanges of digits I to II are pressed over the terminal phalanx of the wing-finger and somewhat deformed. All phalanges of the left pes are seen in dorsal view, except for the ungual of digit I that is seen in lateral aspect. The proximal phalanges lie in direct articulation with their respective metatarsals. In the right pes the phalanges overlie each other and the unguals, with the

exception of digit one, are seen in lateral aspect. The latter ungual is disarticulated and seen in dorsal view.

Digit I. The proximal joint of the basal phalanx of digit I is one third smaller than the distal joint of metatarsal I. The mid-shaft the bone had a constriction, which is now compressed. From there, the bone tapers towards its rounded distal end, which is two thirds the width of the proximal articular face. The phalanx is one fifth the length of the respective metatarsal. The medial third of proximal phalanx II is overlain by the proximal phalanx of digit III such that the diameter of the proximal articular face cannot be seen. The narrowest point of the bone is at the mid-shaft constriction. The distal articular face is a double 'roller' joint with a shallow incision between the condyle.

Digit II. Digit II is one third thicker than at the narrowest circumference at the incision between the condyle of the distal articular face of the basal phalanx. The length of this phalanx equals that of the proximal phalanx of digit I and is equally as robust. The distal terminus of the penultimate phalanx of digit II is damaged, and most of the proximal articulation is hidden below the proximal phalanx of digit II and the terminal wing-finger phalanx. Its length is one third shorter than the phalanx of digit I. On the preserved piece of bone, there is no mid-shaft circumference visible.

Digit III. The proximal phalanx of digit III is approximately one third longer than the proximal phalanx of digit II. The proximal articular face is one third the diameter of the distal articular face of the respective metatarsus and has the same diameter as its distal 'roller' articulation, where both condyles are separated by a deep sulcus. The penultimate phalanx of digit III has half the length of the penultimate phalanx of digit I and about the same maximum with at the proximal articular face. The bone is narrowest at the mid-shaft circumference and towards the proximal and distal articular head expands by one third, whereby the distal articular face is a little smaller than the proximal one.

Digit IV. The proximal phalanx of digit IV is one quarter shorter than the proximal phalanx of digit III and at its proximal articular face it is one third thicker. Again, the proximal diameter of the bone is one third smaller than the distal articulation of the respective metatarsal. The mid-shaft circumference marks the thinnest part of the shaft with half the diameter of that of the proximal articular face. The distal 'roller' joint must have been about one third narrower than the proximal articular face, but the medial condyle is destroyed by compression as is the entire phalanx 2.

Digit V. Basal phalanx V has one fourth the length of basal phalanx IV and is rounded triangular in outline. It is twice as long as it is wide.

Ungual phalanges. The preserved ungual phalanges are of approximately the same size and have half the length of penultimate phalanx of digit I. In dorsal view the unguals have a triangular outline and are twice as long as they are wide shortly distal to the slightly concave proximal margin. The curvature is low with flatly convex dorsal margin in lateral view. The proximal articular face measures one third of the ungual in lateral aspect and extends obliquely from dorsodistally to ventroproximally at an angle of about 100° to the vertical plane. The flexor tubercle is tiny, covering just the proximal fifth of the ungual. The plantar margin of the tubercle is slightly convex curving dorsally into the ungual sole, which is straight or shallowly convex.

Pes as an entity. Considering all the phalanges together and reconstructing the missing parts of the pes, digit II was the longest, being one ungual length longer than digits I and III and likely IV, which were all of nearly the same length (Fig. 12). The fifth pedal digit is by far the shortest with less than one sixth the length of the first pedal digit.

Soft tissues

Despite the exceptional state of preservation of the skeleton, there is little evidence for the preservation of soft tissues, either as impressions (external moulds), as mineralizations or as carbonized residues. However, in a small area adjacent to WP I and II of the left wing a small area of wing membrane is preserved (Fig. 21). It is identified as such on account of its intimate association with the wing phalanges and the presence of fibres lying parallel to the articulated wing bones and here interpreted as aktinofibrils sensu Wellnhofer (1991) (Fig. 21B, C). Preservation appears to be as a carbonized residue with a brown colouration, perhaps hinting at some Fe content. A smaller patch of wing membrane is preserved adjacent to the ulna of the left wing but the aktinofibrils are less distinct here. Individual fibres are continuous and unbranched, but some fine aktinofibrils are intercalated between thicker fibres. The average thickness of the aktinofibrils is ~ 0.1 mm. This is consistent with measurements provided by Unwin and Bakhurina (1994) for *Sordes pilosus* from the Late Jurassic of Kazakhstan and other small sized (2 m or less wingspan) pterosaurs (e.g., Wellnhofer 1987; Bennett 2000, 2016; Kellner et al. 2010; Tischlinger and Frey 2002; Unwin and Martill 2019).

Fig. 21 *Balaenognathus maeuseri* gen. et sp. nov. (NKMB P2011-633): soft tissue preservation. **A** Wing elements with soft tissue preservation under normal light (red frame marks section seen in **B**); **B** UV close-up of **A** (red frame marks section seen in **D**; **C** interpretive drawing of **B**; **D** UV close-up of the section seen in the red frame in **B**
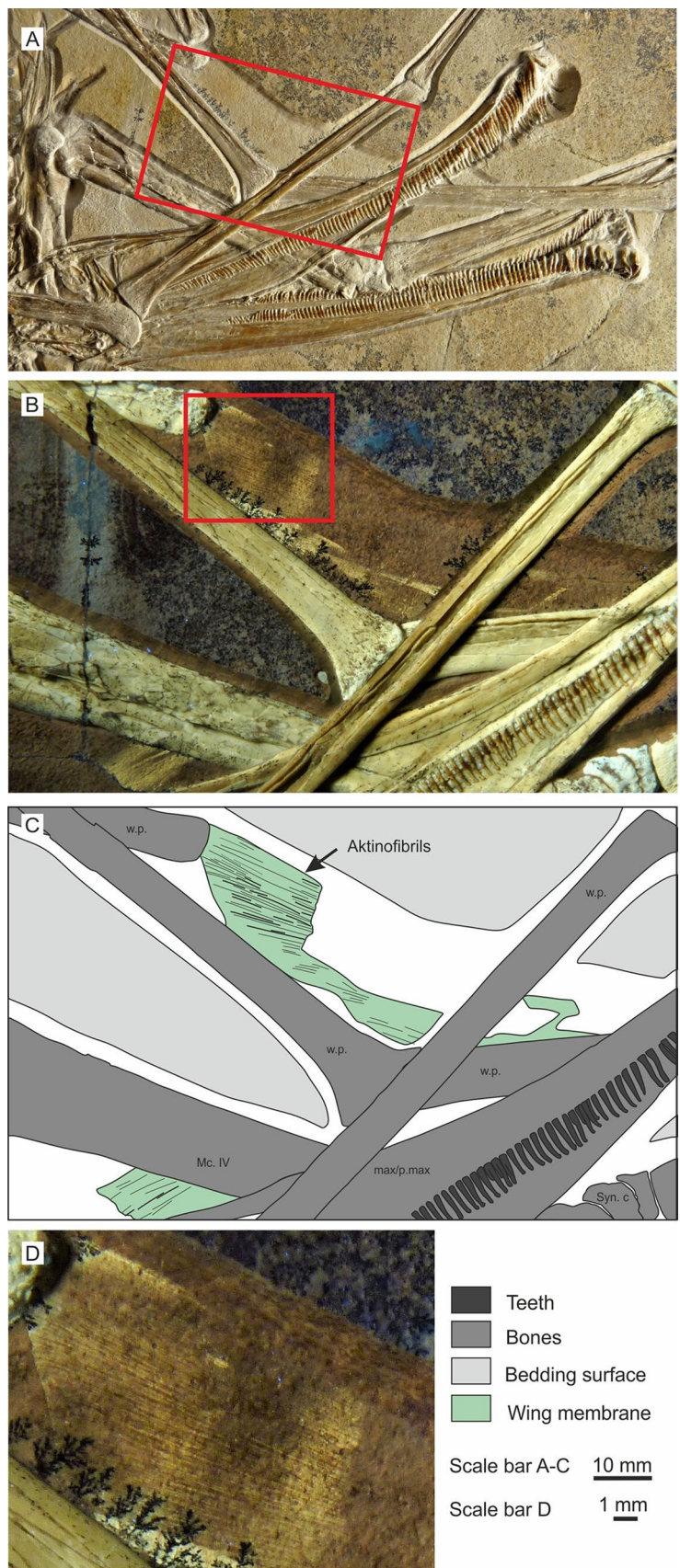
Discussion

Phylogenetic relationship

In a phylogenetic analysis *Balaenognathus* falls within the Ctenochasmatidae where it is the sister taxon to a clade containing *Aurorazhdarcho*, *Gladocephaloideus*, *Feilongus*, *Moganopteryx* and *Lonchodectes* (Fig. 22). This clade, although not well supported, forms a polytomy with well-known ctenochasmatids *Petrodaustro*, *Ctenochasma* and

Gnathosaurus, plus *Eosipterus* and *Liadactylus* (see SI for details of the analysis: For character coding see SI Table 1; for the data matrix see SI Table 2; for the characters list and scoring see SI Table 3).

The Ctenochamatidae Nopcsa, 1928 were a diverse and widely distributed clade of pterodactyloid pterosaurs, first recorded in Europe from the Late Jurassic (Tithonian) Solnhofen Limestone of Bavaria, Germany (Meyer 1833, 1852, 1854) and in the Portlandian of France (Taquet 1972). More recently, their remains have been found in strata as

Fig. 22 Cladogram highlighting the systematic position of *Balaenognathus maeuseri* gen. et sp. nov. with respect to other Pterosauria

Strict consensus of 1863 trees
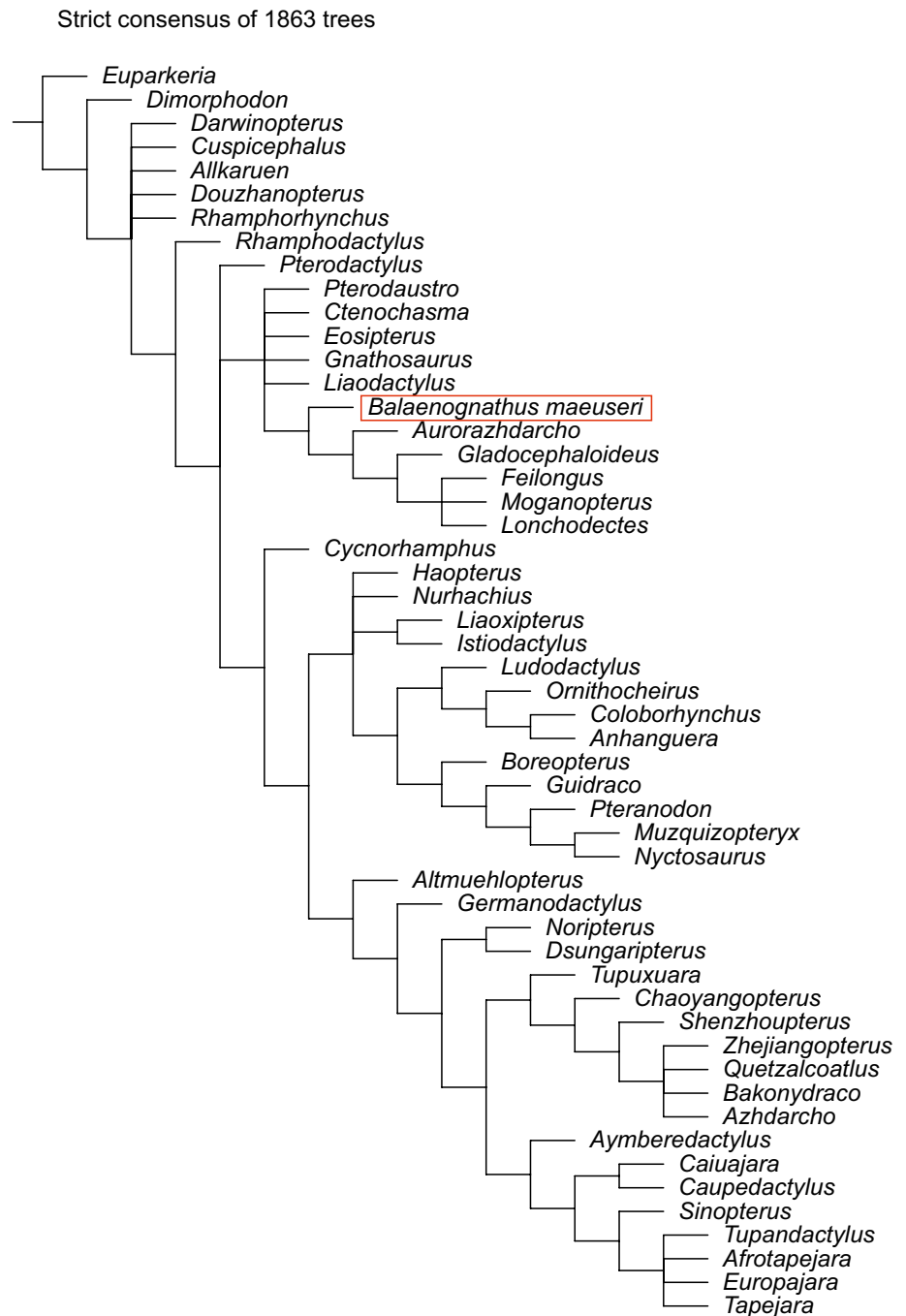
old as Kimmeridgian (this paper) and as young as Early Cretaceous: Jurassic/Early Cretaceous. Ctenochasmatid pterosaurs are reported from North Africa, England, China, Uruguay, Argentina, Chile and North America (Andres and Ji 2008; Bonaparte 1970; Buffetaut and Jeffrey 2012; Dong 1982; Harris and Carpenter 1996; Howse and Milner 1995; Ji and Ji 1997; Lü et al. 2012; Martill et al. 2006; Perea et al. 2018; Sotto et al. 2021; Wang et al. 2006). Ctenochasmatids are typified by large numbers of elongate slender, slightly curved or even recurved interlocking teeth primarily involved in filter-feeding. In one taxon, *Pterodaustro* Bonaparte, 1970 the teeth in the upper jaw are small and somewhat globular, but the teeth of the dentary are among the longest in terms of aspect ratio (l/d) of any tetrapod, and indeed, the most numerous of any tetrapod fossil or extant (Chiappe and Chinsamy 1996). Ctenochamatid skulls are typically elongate, and often gently upwardly curved in the rostrum. Wing spans vary from as small as 250 mm in the smaller examples of *Ctenochasma elegans* (Bennett 1996) to over 2.5 m in the largest form, *Elanodactylus* (Andres and Ji 2008). For *Balaenognathus* the wings span is calculated simply as: span = cor. + hum. + ul. + carp. + mcIv + phs i-iv × 2 = 1.17 m, making it a medium sized ctenochamatid.

Palaeoecology

Filter-feeding in pterosaurs. Filter-feeding among pterosaurs likely evolved from animals that collected food items from the water surface or immediately below without applying a piercing bite. The food item was only held between the teeth and the water drained out when the jaws were lifted. The elongation of the rosette teeth and the reduction of the interdental space as well as the elongation of the jaws enhanced this filter effect. With the elongation of the teeth and the increase in their slenderness, piercing became problematic due to stability problems of the elongate rostrum. As soon as coarse filter-feeding became obligatory, the option for modifying the filter apparatus opened. The rosette teeth could become finer and the tooth rosette enlarged posteriorly. With finer filters, some pterosaur species began to exploit nutrient-rich plankton as food source, with the minimum size of the food particles mirrored by the distance of the teeth. There are several ways filtration can occur: ingesting large volumes of water and ejecting it over a filter, or passively straining food from a natural water current over a filter apparatus, as practiced by many sessile invertebrates (e.g., sabellid worms). Alternatively, filtration can be achieved by actively funneling water into the filter during forwards movement, so-called ram filtration (Simon et al. 2009). Ram filtration, however, works only with the jaws almost closed (e.g., Carey and Goldbogen 2017; Simon et al. 2009).

Feeding mechanisms for Balaenognathus. The dentition of *Balaenognathus* with its numerous interdigitating very slender teeth is strongly indicative of a filter feeder (Figs. 2, 3, 5, 6, 7, 8, 15, 16). The arrangement of the teeth at the end of the jaws and the hooklets on the tooth crowns suggests a unique filter-feeding apparatus previously unknown within the Pterosauria. The teeth of the spatulate part of the jaws do not form a terminal rosette but are short with a near vertical crown forming a funnel-like structure (Figs. 6, 8, 15, 17, 25). The terminal margin of the rostral spatula is edentulous, and even in full possible occlusion there is an aperture allowing nutrient-rich water to flow into the buccal cavity (Figs. 17, 23). In *Balaenognathus* an interdigitation of the teeth beyond about half the tooth length was blocked because of the nubbins and hooklets at the tips of the tooth crowns. Such structures are absent in all other filter-feeding pterosaurs such as *Ctenochasma*, *Gnathosaurus*, *Pterodaustro* (Fig. 24) but a full occlusion was impossible. Unique to *Balaenognathus* is the permanent gape of the anterior third of the rostrum because of the upper jaw being more strongly curved than the lower jaw (Fig. 17 2B) (Note, in *Ctenochasma* the upper jaw is also slightly more curved than the lower [Bennett 2021]). Additionally, the edentulous straight anterior margin of the rostral spatula leaves an opening between the elongated nearly vertical front teeth for the intake of nutrient-rich water. Another feature relevant for the interpretation of the feeding mechanism of *Balaenognathus* is the long rectangular retroarticular process (Figs. 6, 17), which is larger with respect to the mandibular length than in any other filter-feeding pterosaur.

The basic filter mechanism of *Balaenognathus* is functionally evident. Presumably plankton-rich water passed through the aperture formed by the anterior-most part of the rostral spatula and laterally by the longest teeth that together form a sort of funnel (Fig. 23). In the upper jaw most of these elongate teeth are premaxillary teeth of the margin of the rostral spatula. In the mandible, the extent of these elongated teeth is equal to that of the upper jaw where they are also limited to the anterior-most part of the rostral spatula (the 'intake' zone, Fig. 23). For water intake at least the anterior third of the rostrum must have been submerged (Fig. 23A, B). The water flow then passed through the rostral spatula, which converges to form a funnel towards the narrowest part of the rostrum immediately posterior to the spatulate region. Thus, water flow accelerated while further concentrating the food particles (concentration zone, Fig. 23A). Both these zones should have been submerged during feeding in order to allow sufficient intake. The effective angle between the intake part of the rostrum and the filter part would have been about 30° (Fig. 23).

Having passed the funnel constriction in posterior direction, the water flow was divided into two partial flows by the palatine keel that begins to bulge immediately posterior to
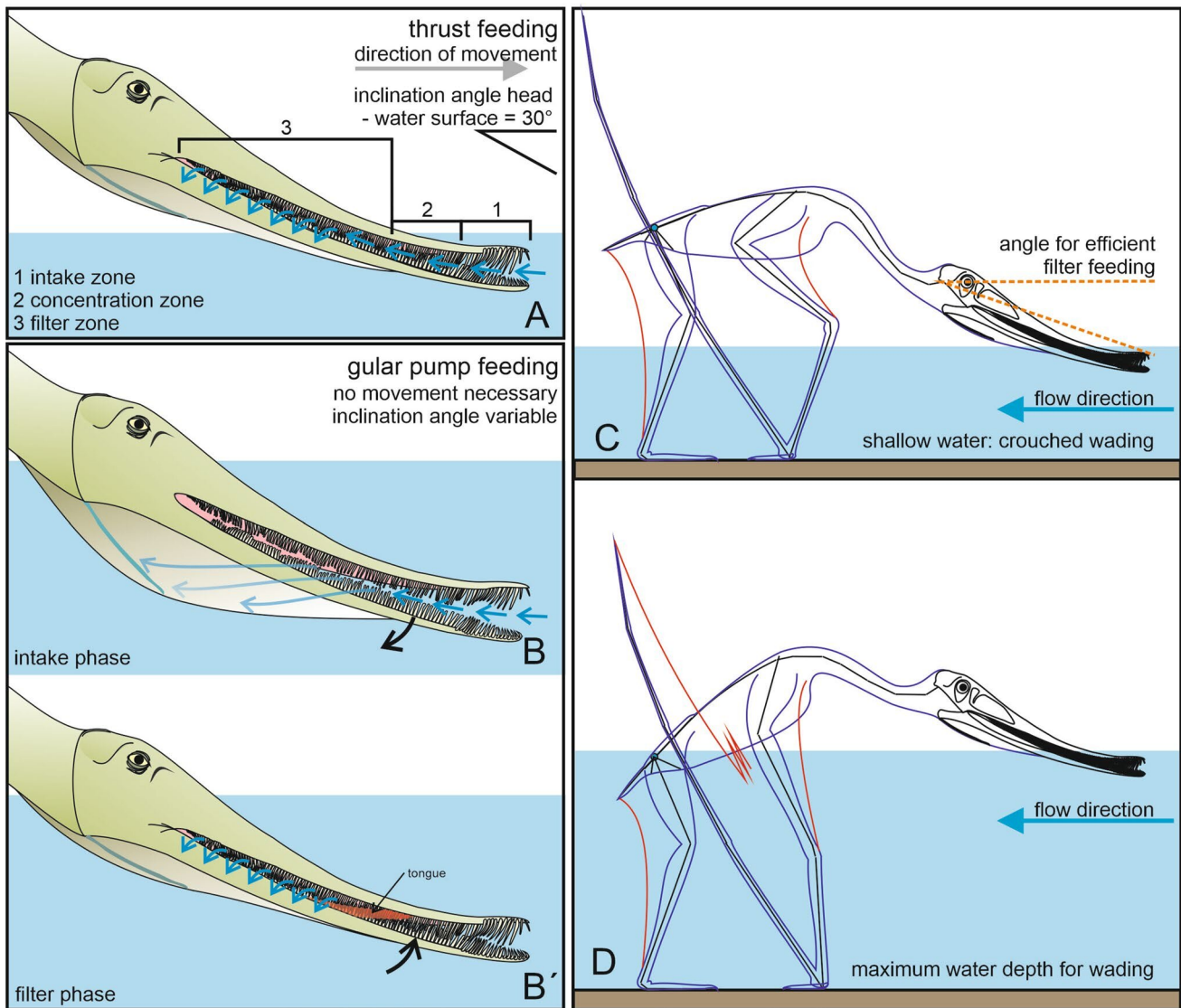
Fig. 23 *Balaenognathus maeuseri* gen. et sp. nov.: possible methods of suspension feeding. **A** Surface thrust feeding; notice that the filter zone should be above the water surface; **B B′**, gular pump feeding, **B**, intake phase, **B′**, filter phase with lingual assistance. **C, D** Range of water depth for passive ram feeding. **C** minimum water level; **D** maximum water level

the funnel (Fig. 23). The keel, the depth of which reaches its maximum with the posterior-most teeth, likely maintained a constant flow of water and thus maintained both the flow speed and volume. At the same time the water flow is directed posterolaterally in the direction of the tooth rows such that the water passes through the dental grid, which retains the food particles (filter zone, Fig. 23A). The gular apparatus and the tongue could have participated to actively control both the speed and direction of the water flow and likely were responsible for passing the concentrated food mass into the pharynx.

An important question is how the inflow of the nutrient-rich water was generated. There are three options to be considered: (1) active ram feeding, (2) passive suspension feeding, and (3) gular pumping (Fig. 23).

Active ram feeding requires a movement of the filter system through the water. This could either be accomplished on the wing (skimming) or while wading (Fig. 24). For *Balaenognathus* skimming would have been physically impossible because the rostral spatula as well as the long front teeth would have caused significant drag that would have become more critical with increased flying speed (see also Humphries et al. 2007 commentary on skimming in pterosaurs, contra Kellner and Campos 2002). Nothing in the skeleton of *Balaenognathus* suggests that such forces could have been compensated. At extremely low flying speeds, which would have been possible, the water flow would have been
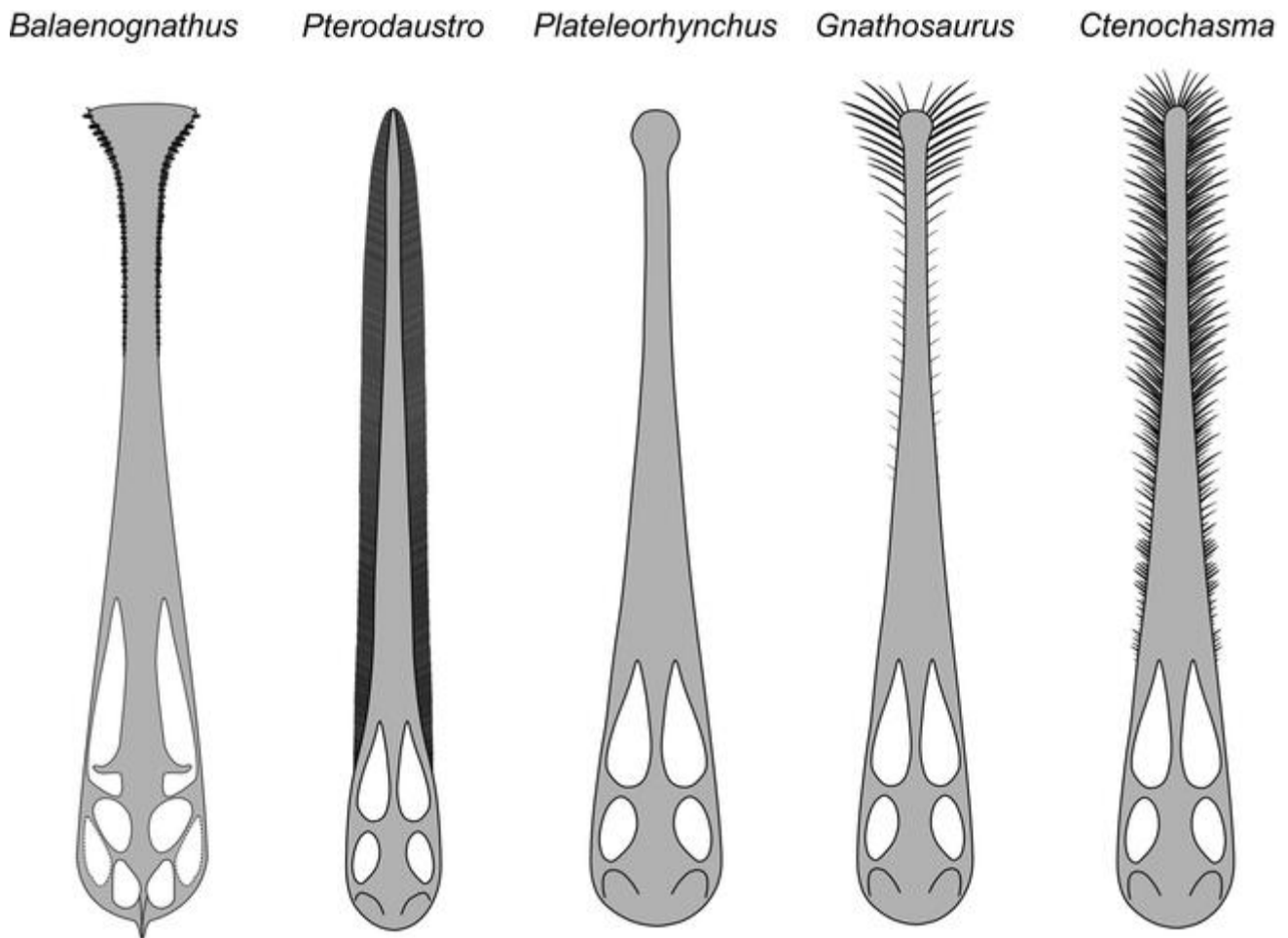
Balaenognathus   Pterodaustro   Plateleorhynchus   Gnathosaurus   Ctenochasma

Fig. 24 *Balaenognathus maeuseri* gen. et sp. nov.: comparative interpretive drawings of the skulls of suspension feeding ctenochasmatoid pterosaurs in dorsal aspect. *Balaenognathus* this paper; *Pterodaustro* based on Bonaparte (1978); *Plateleorhynchus* based on Howse and Milner (1995); *Gnathosaurus* based on specimen JME-SOS 4580; *Ctenochasma* based on (2007 Fig. 2F)

too slow to reach the pharynx. This latter argument also speaks against skimming during wading, especially because the short neck with respect to the skull could not efficiently assist to push the water up the rostrum. Active skimming of any type thus must be precluded as a feeding option for *Balaenognathus*.

Passive suspension feeding could have been an option, despite this feeding method is mostly know from extant invertebrates (e.g., cnidarians, some gastropods (*Viviparus*), some annelids, crinoids, decapod crustaceans, insect larvae (e.g., simuliids). Aerial passive suspension feeders would be spiders with stationary webs. Among vertebrates such kind of suspension feeding is hitherto unknown but would have been an option for *Balaenognathus*. A prerequisite would be nutrient-rich shallow flowing water, e.g., in rivers and creeks, estuaries, and or tidal channels. The morphology of the filter system of *Balaenognathus* would allow such a kind of suspension feeding resembling an eel trap, which is a passive fishing net fixed in flowing water. Eel traps are cylindric baskets containing a row of funnels that direct the path of the fish and at the same time prevent their escape.

The active production of a water current through the mouth of *Balaenognathus* would require an active buccal dilatation system. The large retroarticular process of *Balaenognathus* would be a prerequisite for such a system in offering an adequate attachment surface and a long operational lever for a powerful m. depressor mandibulae (Fig. 17D). However, because of the thickened apices of the tooth crowns, the amplitude of the jaw movement could have only been three or four millimetres in the area of the rostral spatula. Here, the internal surface of the spatula was sufficiently large to produce reasonable suction. A small aperture of the rostral spatula could have prevented the intake of too large food items. Flexible tooth crowns would be an advantage to secure a dense interlock of the opposing tooth rows. However, because of the impossibility of a full jaw occlusion in *Balaenognathus,* the water would have been expelled during jaw adduction. Therefore, in this model, water intake must

Table 1 Table of bones present in specimen NKMB Watt2011/633

Name of element	Aspect	Comment
Skull		
Mandible—both rami	Right lateral, anterior fourth dorsolateral (dentary, angular, articular, massive retroarticular process; left dorsomedial rim (splenial, angular, coronoid, Meckelian canal)	Full dentition retained, partially damaged or displaced (midpart left) but mostly in situ
Premaxilla/maxilla complex	Right lateral	Full dentition retained damaged but in situ (midpart)
Cranium Includes:	Right lateral	Likely complete but obscured by overlying wing phalanx
L. and R. jugals	Right lateral/left medial	Base obscured
L. and R. lacrimals	Right lateral/left medial	Partially obscured by jugals and wing phalanges
R. frontal	Right lateral (fragment of the left in dorsal view?)	
R. nasal	Right lateral	
R. quadrate	Right lateral	
L. quadrate	Posteromedial view	
R. parietal	Lateral view	
?R. squamosal	Lateral view	Obscured by phalanges
L. and R. ceratohyals	Dorsomedial/dorsolateral views	posteriorly in situ, anteriorly slightly depressed
Vertebral column		
CV1	Likely dorsolateral view	Very crushed
CV2	R. lateral view	In tight articulation with CV3
CV3	R. lateral view	In tight articulation with CV4
CV4	R. lateral view	Open articulation with CV5
CV5	R. lateral view	Open articulation with CV6
CV6	R. lateral view	Articulation with CV7 obscured
CV7	R. dorsolateral view	Much obscured by MCIV and crushed
At least 2 notarial vertebrae (posterior ones?)	Dorsal view	Very much obscured by right radius/ulna
Four x posterior thoracic verts clearly visible. In total likely 7 based on transverse processes	Dorsal view	Anterior 3 obscured by right MCIV with only transverse processes visible
Three x lumbar vertebrae	Dorsal view	
Synsacrum (four visible sacrals, a 5th is partially visible (left sacral rib)	Dorsal view	Posterior end covered by right femur
12 caudal vertebrae	R. lateral view	Articulated in two segments
Ribs of the r. side (at least 13)	All views	Some broken, some partially obscured. Seemingly more disarticulated than ribs of the left side, mixed with gastralia
Ribs of the l. side (at least 13)	Mostly seen in posterior view	Lie in overlapping, partially articulated group
Ventral ribs (Gastralia)	Likely dorsal and posterodorsal view	Several finer ribs, tapered at both extremities or with an excavated body are regarded as gastralia
Pectoral girdle		
R. Coracoid	Posterior view	Fully exposed. Not fused with scapula
R./L. scapula	dorsolateral (mostly lateral) / dorsolateral (posterior fourth (mostly dorsal)	Proximal end visible, but mostly obscured by r. ulna and humerus
Sternum	Dorsal	Element poorly exposed and partly obscured by r. humerus
Forelimbs		
R. humerus	Palmar (ventral)	Complete
L. humerus	Palmar (ventromedial)	Proximally obscured by WF Ph 1
R. ulna	Posterior view	
L. ulna	Dorsal view	Partly obscured by rostrum

Table 1 (continued)

Name of element	Aspect	Comment
R. radius	Dorsal view	Mostly obscured by ulna
L. radius	Dorsal view	Partly obscured by rostrum
R. syncarpals		Partially displaced due to over-flexion but still in articular contact; preaxial carpal exposed
L. syncarpals	Dorsal view	Perfectly articulated. Proximal fused, distal separate (sutured)
R. MC I	Dorsal	Only distal part visible
L. MC I	?Dorsal	Mostly obscured by mandibular dentition
R. MC II	Dorsal view	Mostly visible
L. MC II	?	Lies adjacent to MC IV. This may be MC III
R. MC III	Dorsal view	Complete
L. MC III	Dorsal view	Lies adjacent to MC IV. This may be MC II (see above)
R. MC IV	Dorsal view	Entire
L. MC IV	?Posterodorsal view	Entire except for tip of distal 'roller' articulation
R. manus digit 1 Ph. 1		
R. manus digit 1 ungual phalanx		
R. manus digit 2 Ph. 1		
R. manus digit 2 Ph. 2		
R. manus digit 2 ungual phalanx		
R. manus digit 3 Ph. 1		
R. manus digit 3 Ph. 2		
R. manus digit 3 Ph. 3		
R. manus digit 3 ungual phalanx	Dorsal view	
R. WF Ph 1	complete	
L. WF Ph 1	Proximal articular end missing	
R. WF Ph 2	Complete. Dorsal view	Strongly hyperextended
L. WF Ph 2	Complete. Dorsal view	Strongly hyperextended
R. WF Ph 3	Complete. Dorsal view	Slightly hyperextended
L. WF Ph 3	Complete. Dorsal view	Slightly hyperextended
R. WF Ph 4	Complete. Dorsal view	Strongly hyperextended
L. WF Ph 4	Complete. Dorsal view	straight
Pelvic girdle		
R. ilium	Dorsal view	Posterior portion obscured by r. femur
L. ilium	Dorsal view	Anterior part of ant. proc. missing. Posterior part obscured by r. femur
R. prepubis	Medial view	Well exposed
L. prepubis	Medial view	Mostly obscured by sacral vertebrae
R. pubis	R. lateral	Partially obscured by head of r. femur
Right ischium	Right lateral	Anterior portion obscured by r. femur
Left ischium	Medial view	Only posteroventral portion visible
Hindlimbs		
R. femur	Ventral view	
L. femur	Medial view	
R. tibiotarsus	Lateral view	
L. tibiotarsus	lateral view	
R. fibula	Lateral view	
L. fibula	Lateral view	
R. Distal tarsal	Dorsolateral view	
L. Distal tarsal	Dorsolateral view	

Table 1 (continued)

Name of element	Aspect	Comment
R. MT 1	Dorsal view	
L. MT 1	Dorsolateral view	
R. MT 2	Dorsal view	
L. MT 2	Dorsolateral view	
R. MT 3	Dorsal view	
L. MT 3	Dorsolateral view	
R. MT 4	Dorsal view	
L. MT 4	Dorsolateral view	
R. MT 5	Lateral view	
L. MT 5	Lateral view	
R. pedal digit 1, ph. 1	Lateral view	
L. pedal digit 1, ph. 1	Dorsolateral view	
R. pedal digit 1, ph. 2	Lateral view	
L. pedal digit 1, ph. 2	Dorsolateral view	
R. pedal digit 1, ungual phalanx	Lateral view	
L. pedal digit 1, ungual phalanx	Dorsolateral view	
R. pedal digit 2, ph. 1		
L. pedal digit 2, ph. 1		
R. pedal digit 2, ungual phalanx	Dorsal view	
L. pedal digit 2, ungual phalanx		
R. pedal digit 3, ph. 1	Dorsal view	
L. pedal digit 3, ph. 1		
R. pedal digit 3, ph. 2	Dorsal view	
L. pedal digit 3, ph. 2		
R. pedal digit 3, ungual phalanx	R. lateral view	
L. pedal digit 3, ungual phalanx		
R. pedal digit 4, ph. 1		
L. pedal digit 4, ph. 1		
R. pedal digit 4, ph. 2		
L. pedal digit 4, ph. 2		
R. pedal digit 4, ph. 3		
L. pedal digit 4, ph. 3		
R. pedal digit 4, ungual phalanx		
L. pedal digit 4, ungual phalanx		
Ungual of R. MT 5		
Ungual of L. MT 5		

have been assisted by gular dilatatio, n which could have been achieved by depression of the hyal apparatus (Fig. 23B, C). The tongue must then have had the function of a valve that prevented the backflush of water. The tongue may also have assisted in pressing the water through the posterior tooth rows. The gular pump would even be sufficient when the rostrum was completely submerged (Fig. 23C).

Some dabbling ducks (e.g., *Anas* spp.) use a similar pumping mechanism by increasing the distance between the maxillary and mandibular lamellae (lamellar separation) to generate low-pressure inside the buccal cavity, and thus suck nutrient-rich water into the mouth (Sanderson and Wassersug 1990). The jaw depression is powered by m. depressor mandibulae (Fig. 17D) inserting on the long lever of the retroarticular process (Gurd 2006, 2007).

From the cranial anatomy and its dentition, both passive suspension feeding (Figs. 23A, 24) and active rostrogular pumping (Fig. 23B, C) would have been options. Likely both were used depending on the situation, but both could only work in shallow water. Based on ichnofossils, it is suggested that ctenochasmatids did indeed forage in shallow water bodies full of small planktonic prey (Qvarnström et al. 2019).

Table 2 Table of measurements of NKMB Watt2011/633

Element	Measurement mm
Skull length	168.2
Skull height – top cranium to base quadrate	31.13
Mandible length	158.35
Longest tooth crown height	10.80
Shortest tooth crown height	1.90
Cervical vertebrae 1/2 - length	13.13*
CV 3 - length	20.45
CV 4 - length	23.89
CV 5 - length	23.81
CV 6 - length	20.67*
CV 7 - length	22.23*
Presternal lumbar vertebrae 1 - length	8.41
Presternal lumbar vertebrae 2	8.12
Sternum	28.74*
Caudal series (12 verts) total length	32.45
1st caudal vert. – length	2.94
Last (?12th) caudal vert. - length	1.96
Right coracoid - length	37.4
R. scapula - length	>49.87
R. humerus – length	65.60
R. ulna - length	86.79
R. carpus	est. 10.00
R. mc IV	99.13
Wing finger phalange 1 - length	131.63
Wing finger phalange 2 - length	98.65
Wing finger phalange 3 - length	77.16
Wing finger phalange 4 - length	63.04
L. humerus - length	55.99*
L. ulna	92.89
L. mc IV	93.78
L. wing finger phalange 1	118.94*
Wing finger phalange 2 - length	98.43
Wing finger phalange 3 - length	79.03
Wing finger phalange 4 - length	69.63
Ilium – composite length form l and r	46.31*
R. Ischium - length	>15.93*
R. pubis - length	>7.52*
R. prepubis - length	20.18
R. prepubis – distal width	20.65*
R. femur - length	71.00
R. tibia - length	113.68
R. fibula - length	52.13
R. mt 1 - length	34.27
R. mt 2 - length	30.59
R. mt 3 - length	26.93
R. mt 4 - length	22.41
R. mt 5 - length	10.00
L. femur – length	72.71
L. tibia - length	115.29
L. mt 1 - length	23.83
L. mt 2 - length	?
L. mt 3 - length	28.51
L. mt 4 - length	23.70
L. mt 5 - length	9.90
Wingspan cor + h + u + car + mciv + phi-iv x 2	1.168 m

Table 2 (continued)

Measurements were obtained using the measuring function in Corel-DRAWX8 on an enlarged digital photograph. An asterisk suggests some minor uncertainty in the measurement due to incompleteness or an obscuring bone preventing as true length being obtained. >symbol indicates measurement of exposed part of bone only

Conclusions

A Late Jurassic pterosaur from the Wattendorf Plattenkalk of the Torleite Formation of Wattendorf, southern Germany, represents a new genus and species of ctenochasmatid pterosaur, *Balaenognathus maeuseri*. It is diagnosed on three apomorphies: 1, long and slender teeth terminating in a small hook or knob; 2, a truncated edentulous anterior jaw termination, and 3, a tooth count greater than 480. The immense number of fine, slender teeth that interdigitate in occlusion mechanically precludes any mode of feeding other than filter feeding. In a cladistic analysis, *Balaenognathus* nests within the Ctenochasmatidae together with other well-known forms such as *Pterodaustro*, *Ctenochasma* and *Gnathosaurus*; however, the group remains rather unresolved. Within the Ctenochasmatoidea, *Balaenognathus* appears to be a sister taxon to the clade Moganopterinae sensu Longrich et al. (2018) comprising *Aurorazhdarcho*, *Gladocephaloides*, *Feilongus*, *Moganopterus* and *Lonchodectes*. The unique jaw morphology, especially of the anterior terminus of the rostrum reveals a wide, edentulous rostral spatula narrowing posteriorly in the manner of a funnel for the ingress of plankton that was filtered out over its array of interlocking needle-shaped teeth. The function of the hooked tooth crowns remains an enigma, but they appear to have limited the gape of the jaws.

and warm-hearted colleague of a kind that can be scarcely found. In order to preserve his memory, we name the pterosaur described herein in his honour.

Declarations

References

Andres, B., and Q. Ji. 2008. A new pterosaur from the Liaoning Province of China, the phylogeny of the Pterodactyloidea, and convergence in their cervical vertebrae. *Palaeontology* 51 (2): 453–469.

Arratia, G., H.-P. Schultze, H. Tischlinger, G. Viohl, and G. 2015. Solnhofen. *Ein Fenster in die Jurazeit* 1: 7–323 (**Vol.2: 331–620**).

Barthel, K.W., N.H.M. Swinburn, and S. Conway Morris. 1990. *Solnhofen: a study in Mesozoic palaeontology.* Cambridge University Press

Bennett, S.C. 1995. A statistical study of *Rhamphorhychus* from the Solnhofen Limestone of Germany: Year-classes of a single large species. *Journal of Paleontology* 69: 569–580.

Bennett, S.C. 1996. Year-classes of pterosaurs from the Solnhofen Limeston of Germany: Taxonomic and sytematic implications. *Journal of Vertebrate Paleontology* 16: 432–444.

Bennett, S.C. 2000. Pterosaur flight: The role of actinofibrils in wing function. *Historical Biology* 14: 255–284.

Bennett, S.C. 2007. A review of the pterosaur *Ctenochasma*: taxonomy and ontogeny. *Neues Jahrbuch Für Geologie Und Paläontologie – Abhandlungen* 245 (1): 23–31. https://doi.org/10.1127/0077-7749/2007/0245-0023.

Bennett, S.C. 2013a. New information on body size and cranial display structures of *Pterodactylus antiquus*, with a revision of the genus. *Paläontologische Zeitschrift* 87 (2): 269–289. https://doi.org/10.1007/s12542-012-0159-8.

Bennett, S.C. 2013b. The morphology and taxonomy of the pterosaur *Cycnorhamphus*. *Neues Jahrbuch für Geologie und Paläontologie – Abhandlungen* 267: 23–41. https://doi.org/10.1127/0077-7749/2012/0295.

Bennett, S.C. 2016. New interpretation of the wings of the pterosaur *Rhamphorhynchus muensteri* based on the Zittel and Marsh specimens. *Journal of Paleontology* 89 (5): 845–869.

Bennett, S.C. 2021. Complete large skull of the pterodactyloid pterosaur *Ctenochasma elegans* from the Late Jurassic Solnhofen Lithographic Limestones. *Neues Jahrbuch für Geologie und Paläontologie, Abhandlungen* 2021: 283–294.

Bestwick, J., D.M. Unwin, R.J. Butler, D.M. Henderson, and M.A. Purnell. 2018. Pterosaur dietary hypotheses: A review of ideas and approaches. *Biological Reviews* 93 (4): 2021–2048.

Bonaparte, J.F. 1970. *Pterodaustro guinazui* gen. et sp. nov. Pterosaurio de la Formación Lagarcito, Provincia de San Luis, Argentina y su significado en la geologia regional (Pterodactylidae). *Acta Geologica Lilloana* 10: 209–225.

Bonaparte, J.F. 1978. *El Mesozoico de América del Sur y sus tetrápodos*. XXIV, Pterosaurios, crocodilos y sauropodos Jurasicos. Pera Lilloana, Tucumán, Argentina. 415–434

Buffetaut, E., and P. Jeffery. 2012. A ctenochasmatid pterosaur from the Stonesfield Slate (Bathonian, Middle Jurassic) of Oxfordshire, England. *Geological Magazine* 149 (3): 552–556.

Carey, N., and J.A. Goldbogen. 2017. Kinematics of ram filter feeding and beat-glide swimming in the northern anchovy *Engraulis mordax*. *The Journal of Experimental Biology* 220: 2717–2725.

Chiappe, L.M., and A. Chinsamy. 1996. *Pterodaustro's* true teeth. *Nature* 37: 211–212.

Chinsamy, A., L. Codornui, and L. Chiappe. 2008. Developmental growth patterns of the filter-feeder pterosaur, *Pterodaustro guinzui*. *Biology Letters* 4 (3): 282–285.

Cohen, K.M., S.C. Finney, P.L. Gibbard, and J.-X. Fan. 2013. The ICS international chronostratigraphic chart. *Episodes* 36: 199–204.

Collini, C.A. 1784. Sur quelques Zoolithes du Cabinet d'Histoire naturelle de SASE Palatine et de Bavière, à Mannheim. *Acta Academiae Theodoro Palatinae, Mannheim, Pars Physica* 5: 58–103

Dong, Z. 1982. On a new pterosaur (*Huanhepterus quingyangensis*, gen. et sp. nov.) from Ordos, China. *Vertebrata Palasiatica* 20: 115–121.

Fastnacht, M. 2005. Jaw mechanics of the pterosaur skull construction and the evolution of toothlessness. *Unpublished Dissertation thesis am Fachbereich Chemie, Pharmazie und Geowissenschaften der Johannes Gutenberg-Universität in Mainz* 228: pp. A1–142.

Frey, E., H. Tischlinger, M.-C. Buchy, and D.M. Martill. 2003a. New specimens of Pterosauria (Reptilia) with soft parts with implications for pterosaurian anatomy and locomotion. *Geological Society, London, Special Publications* 217: 233–266.

Frey, E., M.-C. Buchy, and D.M. Martill. 2003b. Middle-and bottom-decker Cretaceous pterosaurs: Unique designs in active flying vertebrates. *Geological Society, London, Special Publications* 217: 267–274.

Frey, E., and D.M. Martill. 1998. Soft tissue preservation in a specimen of *Pterodactylus kochi* (Wagner) from the Upper Jurassic of Germany. *Neues Jahrbuch für Geologie und Paläontologie, Abhandlungen* 210: 421–441.

Gurd, D.B. 2006. Filter-feeding dabbling ducks (*Anas* spp.) can actively select particles by size. *Zoology* 109: 120–126.

Gurd, D.B. 2007. Predicting resource partitioning and community organization of filter-feeding dabbling ducks from functional morphology. *The American Naturalist* 169: 334–343.

Hone, D., and M., Habib, M. Lamanna. 2013. An annotated and illustrated catalogue of Solnhofen (Upper Jurassic, Germany) pterosaur specimens at Carnegie Museum of Natural History. *Annals of Carnegie Museum* 82: 165–191.

Howse, S.C.B., and A.R. Milner. 1995. The pterodactyloids from the Purbeck Limestone Formation of Dorset. *Bulletin of the Natural History Museum London (geology)* 51: 73–88.

Harris, J.D., and K. Carpenter. 1996. A large pterodactyloid from the Morrison Formation (Late Jurassic) of Garden Park, Colorado. *Neues Jahrbuch für Geologie und Paläontologie, Monatsheft* 8: 473–484.

Humphries, S., R.H.C. Bonser, M.P. Witton, and D.M. Martill. 2007. Did pterosaurs feed by skimming? Physical modelling and anatomical evaluation of an unusual feeding method. *PLoS Biology* 5 (8): e204. https://doi.org/10.1371/journal.pbio.0050204.

Ji, S., and Q Ji. 1997. Discovery of a new pterosaur in western Liaoning, China. *Acta Geologica Sinica-English Edition* 71 (2): 115–121.

Kaup, J. 1834. Versuch einer Eintheilung der Säugethiere in 6 Stämme und der Amphibien in 6 Ordnungen. *Isis* 3: 311–315.

Kellner, A.W.A. 2003. Pterosaur phylogeny and comments on the evolutionary history of the group. *Geological Society, London, Special Publications* 217: 105–137.

Kellner, A.W.A., and D.A. Campos. 2002. The function of the cranial crest and jaw of a unique pterosaur from the Early Cretaceous of Brazil. *Science* 297: 389–392.

Kellner, A.W., X. Wang, H. Tischlinger, and H., D. de Almeida Campos, D.W. Hone, X. Meng. 2010. The soft tissue of *Jeholopterus* (Pterosauria, Anurognathidae, Batrachognathinae) and the structure of the pterosaur wing membrane. *Proceedings of the Royal Society b: Biological Sciences* 277 (1679): 321–329.

Lü, J.-C. 2003. A new pterosaur: *Beipiaopterus chenianus*, gen. et sp. nov. (Reptilia: Pterosauria) from Western Liaoning Province, China". *Memoir of the Fukui Prefectural Dinosaur Museum* 2: 153–160.

Lü, J., Q. Ji, X. Wei, and Y. Liu. 2012. A new ctenochasmatoid pterosaur from the Early Cretaceous Yixian Formation of western Liaoning, China. *Cretaceous Research* 34: 26–30.

Lü, J.-C., D.M. Unwin, X. Jin, Y. Liu, and Q. Ji. 2010. Evidence for modular evolution in a long-tailed pterosaur with a pterodactyloid skull. *Proceedings of the Royal Society B* 277 (1680): 383–389. https://doi.org/10.1098/rspb.2009.1603.PMC2842655.

Longrich, N.R., D.M. Martill, and B. Andres. 2018. Late Maastrichtian pterosaurs from North Africa and mass extinction of Pterosauria at the Cretaceous-Paleogene boundary. *PLoS Biology* 16 (3): e2001663.

Martill, D.M., E. Frey, C.M. Bell, and G. Chong Diaz. 2006. Ctenochamatid pterosaurs from Early Cretaceous dposits in Chile. *Cretaceous Research* 27: 603–610.

Mäuser, M. 2015. Die laminierten Plattenkalke von Wattendorf in Oberfranken. In *Solnhofen – Ein Fenster in die Jurazeit, eds. G. Arratia, H.P. Schultze, H. Tischlinger, and G. Viohl. 515–535. Munich: Friedrich Pfeil.

von Meyer, C.E.H. 1833. *Gnathosaurus subulatus*, ein Saurus aus den lithographischen Schiefer von Solnhofen. *Museum Senckenbergianum* 1 (3): 1–26.

Meyer, C.E.H., von 1852. *Ctenochasma Roemeri*. *Paläontographica* 2: 82–84, pl. 13

Niebuhr, B., and T. Pürner. 2014. Plattenkalk und Frankendolomit – Lithostratigraphie der Weißjura-Gruppe der Frankenalb (außeralpiner Oberjura, Bayern). *Schriftenreihe der Deutschen Gesellschaft für Geowissenschaften* 83: 5–72.

Nopcsa, F.V. 1928. The genera of reptiles. *Palaeobiologica* 1: 163–188.

Ősi, A., E. Prondvai, and B. Géczy. 2010. The history of Late Jurassic pterosaurs housed in Hungarian collections and the revision of the holotype of *Pterodactylus micronyx* Meyer 1856 (a 'Pester Exemplar'). *Geological Society, London, Special Publications* 343: 277–286.

Perea, D., M. Soto, P. Toriño, V. Mesa, and J.G. Maisey. 2018. A Late Jurassic-? Earliest Cretaceous ctenochasmatid (Pterosauria, Pterodactyloidea): The first report of pterosaurs from Uruguay. *Journal of South American Earth Sciences* 85: 298–306.

Plieninger, F. 1901. Beiträge Zur Kenntnis Der Flugsaurier. *Paläontographica* 48: 65–90.

Qvarnström, M., E. Elgh, K. Owocki, P.E. Ahlberg, and G. Niedzwiedzki. 2019. Filter-feeding in Late Jurassic pterosaurs supported by coprolite contents. *PeerJ* 7: e7375. https://doi.org/10.7717/peerj.7375.

Sanderson, S.L., and R. Wassersug. 1990. Suspension-feeding vertebrates. *Scientific American* 262 (3): 96–102.

Schweigert, G. 2007. Ammonite biostratigraphy as a tool for dating Upper Jurassic lithographic limestones from South Germany – first results and open questions. *Neues Jahrbuch Für Geologie Und Paläontologie, Abhandlungen* 245: 117–125.

Simon, M., M. Johnson, P. Tyack, and P. Madsen. 2009. Behaviour and kinematics of continuous ram filtration in bowhead whales (*Balaena mysticetus*). *Proceedings of the Royal Society B. Biological Sciences* 276: 3819–3828. https://doi.org/10.1098/rspb.2009.1135.

Soto, M., F. Montenegro, P. Toriño, V. Mesa, and D. Perea. 2021. A new ctenochasmatid (Pterosauria, Pterodactyloidea) from the late Jurassic of Uruguay. *Journal of South American Earth Sciences* 111: 103472.

Taquet, P. 1972. Un crane de *Ctenochasma* (Pterodactyloidea) du Portlandien inferieur de la Haute-Marne, dans les collections du Musee de St-Dizier. *Comptes Rendus De L'académie Des Sciences* 174: 362–364.

Tischlinger, H. 2002. Der Eichstätter *Archaeopteryx* im langwelligen UV-Licht. *Archaeopteryx* 20: 21–38.

Tischlinger, H. 2015. Arbeiten mit ultraviolettem Licht (UV). In *Solnhofen - Ein Fenster in die Jurazeit*, eds. G. Arratia, H.-P. Schultze, H. Tischlinger, and G. Viohl. 109–113. Munich: Friedrich Pfeil

Tischlinger, H., and G. Arratia. 2013. Ultraviolet light as a tool for investigating Mesozoic fishes, with a focus on the ichthyofauna of the Solnhofen archipelago. *Mesozoic Fishes* 5: 549–560.

Tischlinger, H., and E. Frey. 2002. Ein *Rhamphorhynchus* (Pterosauria, Reptilia) mit ungewöhnlicher Flughauterhaltung aus dem Solnhofener Plattenkalk. *Archaeopteryx* 20: 1–20.

Tischlinger, H., and E. Frey. 2013. Ein neuer Pterosaurier mit Mosaikmerkmalen basaler und pterodactyloider Pterosauria aus dem Ober-Kimmeridgium von Painten (Oberpfalz, Deutschland). *Archaeopteryx* 31: 1–14.

Tischlinger, H., and E. Frey. 2015. Flugsaurier (Pterosauria). In *Solnhofen - Ein Fenster in die Jurazeit,* eds. Arratia, G., H.-P. Schultze, H. Tischlinger, and G. Viohl, 459–480. Munich: Friedrich Pfeil

Unwin, D.M. 1995. Preliminary results of a phylogenetic analysis of the Pterosauria (Diapsida: Archosauria). In *Sixth symposium on Mesozoic Terrestrial Ecosystems and Biota, Short Papers, 1995*, ed. A. Sun and Y. Wang, 60–72. Beijing: China Ocean Press.

Unwin, D.M. 2003. On the phylogeny and evolutionary history of pterosaurs. *Geological Society, London, Special Publications* 217: 139–190.

Unwin, D.M., and N.N. Bakhurina. 1994. *Sordes pilosus* and the nature of the pterosaur flight apparatus. *Nature* 371: 62–64.

Unwin, D.M., and D.M. Martill. 2019. No protofeathers on pterosaurs. *Nature Ecology and Evolution*. https://doi.org/10.1038/s41559-020-01308-9.

Vidovic, S.U., and D.M. Martill. 2014. *Pterodactylus scolopaciceps* Meyer, 1860 (Pterosauria, Pterodactyloidea) from the Upper Jurassic of Bavaria, Germany: the problem of cryptic pterosaur taxa in early ontogeny. *PLoS ONE* 9 (10): e110646.

Völkl-Costantini, P., and P. Völkl. 2013. Sensationeller Flugsaurierfund Aus Wattendorf. *Der Präparator* 59: 30–35.

Wang, X., A.W.A. Kellner, Z. Zhou, and D.A. Campos. 2006. A new pterosaur (Ctenochasmatidae, Archaeopterodactyloidea) from the Lower Cretaceous Yixian Formation of China. *Cretaceous Research* 28: 245–260.

Wellnhofer, P. 1970. Die Pterodactyloidea (Pterosauria) der Oberjura-Plattenkalke Süddeutschlands. *Abhandlungen der Mathematisch-Physikalischen Klasse der Königlich Bayerischen Akademie der Wissenschaften* 141: 1–133.

Wellnhofer, P. 1987. New crested pterosaurs from the Lower Cretaceous of Brazil. *Mitteilungen der Bayerischen Staatssammlung für Paläontologie und Historische Geologie* 27: 175–186.

Wellnhofer, P. 1991. *The illustrated encyclopedia of pterosaurs*, 192. London: Salamander Books.

Witton, M. 2014. *Pterosaurs: natural history, evolution, anatomy*. Princeton: Princeton University.

Zeiss, A. 1977. Jurassic stratigraphy of Franconia. *Stuttgarter Beiträge zur Naturkunde (b)* 31: 1–32.

Zhou, C.F., K.Q. Gao, H. Yi, J. Xue, Q. Li, and R.C. Fox. 2017. Earliest filter-feeding pterosaur from the Jurassic of China and ecological evolution of Pterodactyloidea. *Royal Society Open Science* 4 (2): 160672.